Shell Model Monte Carlo for Gamow-Teller strengths and two-neutrino double beta decay

Thesis by

Radha Pillapakkam Bahukutumbi

In Partial Fulfillment of the Requirements

for the Degree of

Doctor of Philosophy

California Institute of Technology

Pasadena, California

1996

(Submitted May 16, 1996)

Acknowledgements

Kellogg has been a very pleasant place for me to work in and for that I must thank the people who work here.

Steve Koonin has been incredibly patient with me and I have learnt a lot from him. His apparent calm when seemingly catastrophic situations arose has taught me much about problem solving. Valuable advice from him is greatly appreciated. Karlheinz is a good friend and has taught me a great deal of nuclear physics. Those frequent trips to Starbucks have been particularly enjoyable. I have benefitted greatly from discussions with Petr Vogel who has made physics tremendously entertaining for me. I have learnt many things from all these people and for that I must thank them.

I must also thank other members of the SMMC group who have provided me with useful perspective on high performance computing and problems in nuclear structure. Michael has been quite a sport in putting up with the vagaries of his office mate. Life at Caltech has been all the more fun with Mitra, Moira and Alycia.

Finally, my sincere thanks to Satya, Sudha, Amma and Appa for their moral support and Hari for being such a card.

Abstract

In this thesis, a method to calculate two-neutrino double beta decay matrix elements employing the Shell Model Monte Carlo is presented. This method is validated against direct-diagonalization for the decay of ^{48}Ca. The first realistic calculation of the nuclear matrix element within the shell model for ^{76}Ge is performed; the result is in reasonable agreement with experiment.

The sensitivity of the shell model results to the nuclear Hamiltonian has been studied for the case of ^{48}Ca where the Hamiltonian used is known to be an optimal one. While one cannot make the nuclear matrix element arbitrarily small, the uncertainty in certain pieces of the Hamiltonian such as the monopole isovector pairing, provides room for at least a factor of two in the matrix element (and hence a factor of four in the half-life) from such calculations.

A Maximum Entropy method to obtain realistic strength functions from imaginary time response functions has been applied to Gamow-Teller response functions calculated using the Shell Model Monte Carlo and the results are validated against direct-diagonalization and experiment.

Future prospects for double beta decay calculations and astrophysical applications of the Gamow-Teller strength functions are briefly discussed.

Contents

List of Figures

List of Tables

Chapter 1 Introduction

The question of the neutrino mass has been an issue since 1930 when Pauli proposed the existence of a light, electrically neutral particle as a way of conserving energy in beta decay. Subsequently, it became apparent from Fermi's theory of beta decay that the mass of the neutrino must be very small compared to the mass of the electron. Since then the search for a neutrino mass has taken several forms. Direct searches involving the kinematics of weak decays have set limits of a few eV from nuclear beta decays. Indirect searches include looking for neutrino oscillations, zero-neutrino double beta decay etc. Anomalies like the solar neutrino problem and the atmospheric neutrino problem may be indicators for a neutrino mass and significant experimental effort is being expended in building neutrino detectors to study these problems. Astrophysical processes allow for setting bounds on neutrino masses, for instance from data on neutrino bursts from supernovae. Searches based on double beta decay have reached a limit of about 0.7 eV for the electron neutrino mass and are expected to reach better limits by about a factor of two in the next several years.

The two-neutrino (2ν) mode of double beta decay was first postulated by Maria Meyer [1] in 1935 shortly after Fermi's theory of β decay appeared and was observed directly for the first time very recently in 1987 [2]. In 1939, Furry [3] proposed the existence of the zero-neutrino (0ν) mode which has not been observed yet.

Prior to 1957 it was believed that a choice of whether the neutrino is Dirac (*i.e.* $\nu_e \neq \bar{\nu}_e$) or Majorana (*i.e.* $\nu_e \equiv \bar{\nu}_e$) could be made. Then in 1955, Ray Davis' null result [4] of anti-neutrinos inducing a reaction like Eq. (1.2) on ^{37}Cl was interpreted as proof that the neutrino was not a Majorana particle. The 0ν

decay, *i.e.*, the following set of decays,

$$n \rightarrow p + e^- + \bar{\nu}_e, \tag{1.1}$$

$$n + \nu_e \rightarrow p + e^-. \tag{1.2}$$

can take place if the neutrino is Majorana.

With the discovery of parity violation [5] in weak interactions in 1957 the Davis experiment had to be reinterpreted and it became apparent that the nature of the electron neutrino was still in question. The reactions for 0ν decay were recognized to be,

$$n \rightarrow p + e^- + \bar{\nu}_e^{RH}, \tag{1.3}$$

$$n + \nu_e^{LH} \rightarrow p + e^-. \tag{1.4}$$

Thus, even if the neutrino were Majorana this decay could not take place because of the wrong handedness of the emitted anti-neutrino.

It was then recognized that if the neutrinos were Majorana (*i.e.*, interpreting the neutrino in Eq. (1.3) and Eq. (1.4) to be different helicity states of an identical particle, and this helicity mismatch was not complete) then 0ν decay could take place [6]. The latter could be achieved if the neutrino has a mass (*i.e.* one can always find a frame where its helicity is reversed, in the extreme case) and/or if there exist some admixtures of right-handed leptonic current coupling to the hadronic current. More recently, it has been recognized that neutrino mass mixing is necessary for right-handed currents to occur and thus, no zero-neutrino $\beta\beta$ decay occurs if all neutrinos are massless [7].

The standard model of weak interactions has so far been a very robust theory. In this model, neutrinos are massless and there are no right-handed charged currents. Thus, zero-neutrino $\beta\beta$ decay can occur only in extensions of the standard

model of electroweak theory and intense modern interest in $\beta\beta$ decay stems from this understanding of the 0ν decays as a useful probe of physics beyond the standard model and that they can even be used to set constraints on grand unified theories.

Experimental searches for $0\nu\beta\beta$ decays require a sagacious choice of the candidate. The half-life that such searches need to target is one of the crucial factors to be considered. Thus, reliable theoretical calculations of decay rates are an important input to experiments. In addition since the deduction of the neutrino mass or the relevant coupling constants from experimental half-lives relies on theoretically calculated nuclear matrix elements, one must be able to describe the nuclear structure relevant for this decay correctly for a reliable interpretation of limits on neutrinoless decays. The 2ν mode because it has been observed, is a useful test of the relevant nuclear physics for 0ν decay. The nuclear matrix elements are similar, thus testing at least some aspects of the nuclear structure important for the 0ν mode. Not the least of all, the calculation of the nuclear matrix element for the 2ν decay is a challenging nuclear structure problem in itself. The calculation of this quantity and other related nuclear structure issues is the subject of this thesis.

In Chapter 1, I provide a brief review of the $2\nu\beta\beta$ decay, mentioning the assumptions that go into calculating the decay rates. I also discuss various nuclear structure issues that arise in calculating the 2ν matrix element. Chapter 2 describes the numerical methods, *i.e.*, the Shell Model Monte Carlo (SMMC), used to calculate Gamow-Teller strength functions and the 2ν matrix element. In Chapter 3, I validate these methods against direct-diagonalization and discuss results of the $\beta\beta$ decay of ^{76}Ge. Finally, I summarise this work and look at future directions that such calculations might take for $\beta\beta$ decay.

Chapter 2 Review

Double beta ($\beta\beta$) decay is the rare process by which a nucleus (A, Z) can decay into a daughter nucleus $(A, Z \pm 2)$ because of the emission of two electrons or positrons with the practical requirement that single beta decays of these nuclei are suppressed either because they are energetically unfavourable or because of angular momentum considerations.

$\beta\beta$ decay can be principally classsified into two modes. One of these is the two-neutrino (2ν) mode,

$$(A, Z) \rightarrow (A, Z + 2) + e_1^- + e_2^- + \bar{\nu}_1 + \bar{\nu}_2 \tag{2.1}$$

which takes place with the emission of two electrons and two neutrinos and is subject to the condition $M(A, Z) > M(A, Z + 2)$. This mode occurs as a second order process in the standard model and is therefore independent of a small possible neutrino mass. In addition, analogous decays involving the decrease of the nuclear charge accompanied by positron decay or bound electron capture may also occur, *i.e*,

$$\begin{aligned} &(A, Z) \rightarrow (A, Z - 2) + e_1^+ + e_2^+ + \nu_1 + \nu_2, \\ &(A, Z) + e_b^- \rightarrow (A, Z - 2) + e^+ + \nu_1 + \nu_2, \\ &(A, Z) + e_b^- + e_b^- \rightarrow (A, Z - 2) + \nu_1 + \nu_2, \end{aligned} \tag{2.2}$$

with the requirements $M(A, Z) > M(A, Z - 2) + 4m_e$, $M(A, Z) > M(A, Z - 2) + 2m_e + B_e$, and $M(A, Z) > M(A, Z - 2) + 2B_e$ respectively (where $M(A, Z)$ is the atomic mass of the nucleus with A nucleons and Z protons and B_e is the binding energy of the bound electron e_b^-). Thus, the decays in Eq. (2.2) have more

stringent energy requirement conditions than the decay where the nuclear charge increases and are expected to be rarer, and hence more difficult to observe. We will restrict our discussion of 2ν decay to those accompanied by the emission of electrons. The zero-neutrino (0ν) mode,

$$(A, Z) \rightarrow (A, Z+2) + e_1^- + e_2^- \tag{2.3}$$

or

$$(A, Z) \rightarrow (A, Z-2) + e_1^+ + e_2^+ \tag{2.4}$$

cannot occur within the standard model, requires the existence of a neutrino mass and admixtures of right-handed currents in weak interactions, and violates lepton number conservation.

Other mechanisms for 0ν decay have been postulated through various extensions of the standard model of electroweak theory [8]. These involve the emission of one or more particles called Majorons, χ, in addition to two electrons, *i.e.*, the modes $(0\nu, \chi)$ or $(0\nu, \chi\chi)$. These Majorons may or may not carry a leptonic charge (and accordingly these decays may or may not conserve lepton number). One crucial constraint on such models comes from e^+e^- collisions at LEP in $CERN$. The precise width of the Z^0 measured in this experiment sets a limit on the rate of Z^0 decay into light scalars and thus the coupling constant in such models. Hence, any model that has an appreciable rate for this decay of the Z^0 can be ruled out. The spectral shapes of the summed-electron energy for the two electrons and single electron spectrum can, of course, be calculated in such models and thus such experimental signatures can be used to set constraints on the mechanism for the zero-neutrino decay. For instance, even though the (0ν) and the $(0\nu, \chi)$ (where χ is a light boson coupling to the neutrinos) have the same matrix elements mediating the decays they have very different experimental signatures. The energy released is distributed over the two observed electrons (neglecting nuclear recoil)

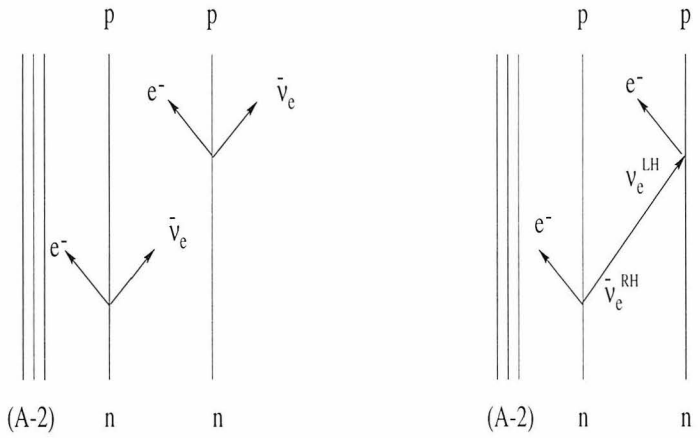

(a) (b)

Figure 2.1: Two-nucleon mechanisms for $\beta\beta$ decay: The figure on the left shows 2ν decay and the figure on the right shows the 0ν decay.

in the former resulting in a summed-electron spectrum that is peaked at the end point energy and over the two electrons and the majoron (which is not observed in the decay and can carry off some energy) making only the maximum of the summed-energy equal to the energy released. (see next section)

Shown in Fig. (2.1) are the two-nucleon mechanisms for $2\nu\beta\beta$, $0\nu\beta\beta$ decays The 2ν decay can proceed through the figure on the left where the states in the intermediate nucleus are virtual. The 0ν decay decay requires a mixing of left and right handedness and can occur through the right figure.

2.1 2ν decay rates

2ν decay can be expressed in terms of sequential single beta decay transitions through virtual intermediate states. Starting with the standard model of weak

interactions (*i.e.*, massless neutrinos and only $V-A$ coupling) one can write an effective Lagrangian in terms of the proton and neutron fields. Then, in the non-relativistic reduction of the hadronic current one retains only the leading order in $\frac{1}{m_N}$ (m_N is the nucleon mass) in the Fermi $\sum_i \tau_i^-$, and the Gamow-Teller (GT) operator, $\hat{\mathbf{G}}= \sum_i \boldsymbol{\sigma}_i \tau_i^-$ (where the sum is over the nucleons in the nucleus) and then in addition retains only the dominant GT operator. The Fermi operator vanishes for transitions involving states of different isospin and isospin mixing is very small in the ground states of nuclei. Thus, the Fermi operator is non-zero only to the extent that the Coulomb interaction mixes the ground state and high-lying states of different isospin. One source of experimental information concerning the validity of this expectation comes from data on $0^+ \rightarrow 0^+$ beta decays. From studies on $\Delta T = 1$ decays, the amount of isospin mixing needed to explain the transition rates does not exceed even a few tenths of a percent.

One is interested in the decay of the ground state of the initial nucleus which has $J^\pi = 0^+$. The double GT operator then excites only 0^+, 1^+, and 2^+ states in the final nucleus. Taking into account the identity of the two electrons and neutrinos emitted, one obtains for the differential rate between the ground states of the initial and final nucleus [9],

$$
\begin{aligned}
d\omega \;\sim\; & \frac{(G_F cos\theta_c)^4 g_A^4}{64\pi^7} \mathcal{F}(\mathrm{Z},\epsilon_1)\mathcal{F}(\mathrm{Z},\epsilon_2) k_1^2 k_2^2 dk_1 dk_2 dcos\theta \nu_1^2 \nu_2^2 d\nu_1 \\
& \frac{1}{3}\sum_{mm\prime}(K_m K_{m\prime} + L_m L_{m\prime} + \frac{1}{2}K_m L_{m\prime} + \frac{1}{2}K_{m\prime} L_m \\
& -\frac{1}{3}(2K_m K_{m\prime} + 2L_m L_{m\prime} + \frac{5}{2}K_m L_{m\prime} + \frac{5}{2}K_{m\prime} L_m)(\vec{\beta}_1 \cdot \vec{\beta}_2))m_m^{2\nu}
\end{aligned}
\tag{2.5}
$$

where G_F is the weak coupling constant obtained from muon decay ($G_F \approx 10^{-5}/M_p^2$;$M_p$ is the proton mass), θ_c is the Cabbibo angle ($\cos\theta_c \sim 0.9737$), g_A is the axial-vector coupling constant measured from the free neutron decay ($g_A = 1.26$), ϵ_i and k_i, $i = 1, 2$, are the energies and three-momenta of the outgo-

ing electrons, $\beta_i = k_i/\epsilon_i$, ν_i are the neutrino energies, and θ is the angle between the electrons. The $\mathcal{F}(\mathrm{Z},\epsilon_i)$ are the Coulomb corrections to the outgoing electron wavefunction evaluated in the field of the final nucleus of charge Z and can be obtained from the ratio of the scattering solution to the Dirac equation to a plane wave, evaluated at the nuclear surface for $\mathcal{F}(\mathrm{Z},\epsilon_i)$ for a qualitative study. A more detailed evaluation taking into account a realistic nuclear charge distribution and atomic screening and numerically integrating the Dirac equation is necessary to be quantitative about decay rates [10]. Then, one assumes that the outgoing electrons are in a s-wave. The indices "m" and "$m\prime$" label the 1^+ state in the intermediate nucleus of energy E_m and the energy denominators K_m and L_m are

$$K_m = \frac{1}{E_m + \epsilon_1 + \nu_1 - E_i^0} + \frac{1}{E_m + \epsilon_2 + \nu_2 - E_i^0} \tag{2.6}$$

$$L_m = \frac{1}{E_m + \epsilon_1 + \nu_2 - E_i^0} + \frac{1}{E_m + \epsilon_2 + \nu_1 - E_i^0}$$

and $m_m^{2\nu}$ is,

$$m_m^{2\nu} = \langle 0_f^+|\hat{\mathbf{G}}|1_m^+\rangle \cdot \langle 1_m^+|\hat{\mathbf{G}}|0_i^+\rangle. \tag{2.7}$$

From Eq. (2.5) it is evident that the outgoing electrons are emitted preferentially back-to-back with an opening angle distribution of $(1 - \vec{\beta}_1 \cdot \vec{\beta}_2)$.

Replacing the lepton energies in Eq. (2.6) by some average value, *i.e.*, writing $\epsilon_1 + \nu_1 = \epsilon_2 + \nu_2 = (E_i^0 - E_f^0)/2 = T_0/2$ and using $K_m \sim L_m$ one obtains an expression for the rate after performing the integral over the angle between the electrons as,

$$\omega = \frac{\ln(2)}{T_{1/2}} = A_{GT} g_A^4 |M^{2\nu}|^2 \tag{2.8}$$

where

$$A_{GT} = \frac{(G_F cos\theta_c)^4}{64\pi^7} \int_{m_e}^{T_0} \mathcal{F}(\mathrm{Z},\epsilon_1)|k_1|\epsilon_1 d\epsilon_1 \tag{2.9}$$

$$\int_{m_e}^{T_0-\epsilon_1} \mathcal{F}(\mathrm{Z},\epsilon_2)|k_2|\epsilon_2 d\epsilon_2 \int_0^{T_0-\epsilon_1-\epsilon_2} \nu_1^2\nu_2^2 d\nu_1$$

and

$$M^{2\nu} = \sum_m \frac{\langle 0_f^+|\hat{\mathbf{G}}|1_m^+\rangle \cdot \langle 1_m^+|\hat{\mathbf{G}}|0_i^+\rangle}{E_m - (E_i^0 + E_f^0)/2} \tag{2.10}$$

is the nuclear matrix element for $2\nu\beta\beta$ decay.

The dependence of the phase space on the energy release in the decay can be obtained from dimensional considerations. However, a detailed dependence becomes transparent upon performing the integrals in Eq. (2.9). Using the Coulomb correction factor introduced by Primakoff and Rosen [6] which is sufficient to demonstrate a qualitative dependence as,

$$\mathcal{F}(\mathrm{Z},\epsilon_i) = \frac{\epsilon_i}{k_i}\frac{2\pi\alpha\mathrm{Z}}{1-e^{-2\pi\alpha\mathrm{Z}}} \tag{2.11}$$

where α is the fine structure constant, one obtains upon substituting this into Eq. (2.9) the dependence of the rate on the end point energy of the spectrum as

$$\omega \sim T_0^7(1 + \frac{T_0}{2} + \frac{T_0^2}{9} + \frac{T_0^3}{90} + \frac{T_0^4}{1980}). \tag{2.12}$$

In contrast, the 0ν decay has a two-lepton final state and an energy dependence of the phase space as T_0^5 with the summed-electron spectrum as a distinguishable δ-function peak as the end point energy (Fig. 2.2). The $(0\nu,\chi)$ decay has a continuous energy spectrum peaked approximately at three quarters of the decay energy, T_0 with an energy dependence of T_0^7 for the phase space. This very different phase space dependence on the end point energy for the various modes of decay results in candidates with a smaller Q-value having an enhanced 0ν rate relative to the 2ν decay and thus such candidates may be preferable for 0ν searches.

The quantity of interest to experiment is the single and two-electron spectrum. The former can be obtained by performing the integral in Eq. (2.9) over $d\epsilon_2$ and

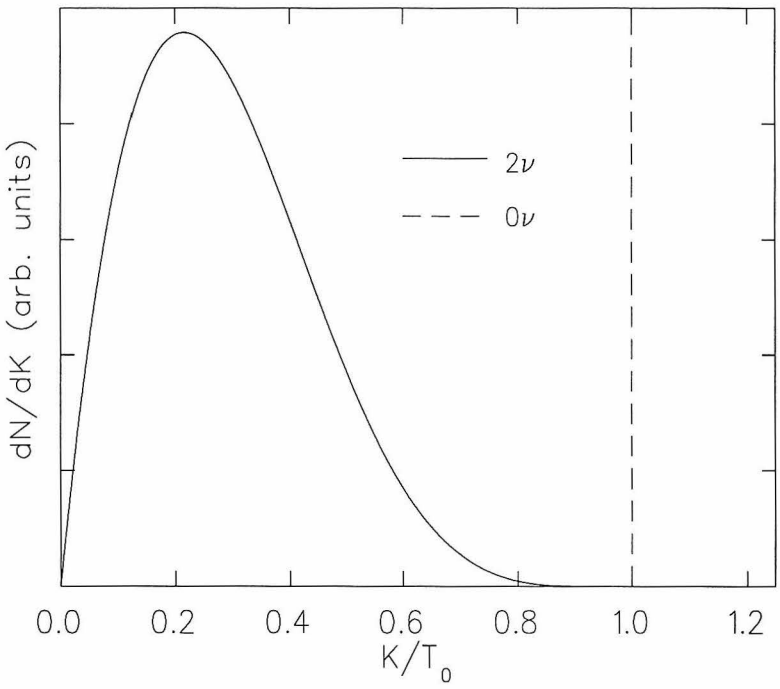

Figure 2.2: Schematic summed-electron spectra for two different modes of $\beta\beta$ decay. The solid curve represents 2ν decay, and the dashed line gives the (0ν) decay. Each spectrum is scaled arbitrarily for convenience.

$d\nu_1$ as,

$$\frac{dN}{d\epsilon} \sim (\epsilon+1)^2(T_0-\epsilon)^6[(T_0-\epsilon)^2+8(T_0-\epsilon)+28] \tag{2.13}$$

and the summed-electron spectrum can be obtained by changing variables in Eq. (2.9) to $(\epsilon_1+\epsilon_2)$ and $(\epsilon_1-\epsilon_2)$ and integrating over the latter. If K is the summed-electron energy, $K=\epsilon_1+\epsilon_2$, then the summed-electron spectrum is

$$\frac{dN}{dK} \sim K(T_0-K)^5[1+2K+\frac{4K^2}{3}+\frac{K^3}{3}+\frac{K^4}{30}]. \tag{2.14}$$

In summary, one can write the rate, Eq. (2.8) as a product of two quantities, one being the phase space factor, $[G^{2\nu}]^{-1} = A_{GT}g_A^4$, which is numerically calculable and the other the nuclear matrix element, $M^{2\nu}$, (Eq. (2.10)), dependent only on the nuclear structure and calculable using models of nuclear structure. In this work, we will use the tabulated values of $[G^{2\nu}]^{-1}$ from Ref [10] (taking into account that these tabulated phase space factors use $g_A = 1.26$ and give a matrix element in units of inverse electron mass).

2.2 Nuclear structure aspects

Two-neutrino decay can be observed principally due to the pairing force. This force prefers to couple pairs of like nucleons to angular momentum zero and can be parametrized as $\delta \approx \pm 12/A^{1/2}$ for even-even (odd-odd) nuclei and $\delta \approx 0$ for odd A nuclei. Thus, from the mass parabola for isobars

$$M(Z,A) \approx const + 2b_{symm}\frac{(A-2Z)^2}{4A^2} + \frac{b_{coul}Z^2}{A^{1/3}} + \delta \tag{2.15}$$

where $b_{symm} \approx 50$ MeV, is the symmetry energy coefficient and $b_{coul} \approx 0.7$ MeV, is the coulomb energy coefficient, one sees that even-even nuclei form one parabola and odd-odd nuclei form another parabola at higher mass. Thus, a situation (like the one shown for ^{76}Ge in Fig. (2.3)) can arise where it becomes energetically

favorable for an even-even nucleus (which is stable against single beta decay) to decay to a nearby even-even nucleus (which is also stable against single beta decay) through an odd-odd nucleus, thus undergoing double beta decay.

An exhaustive search in the mass tables reveals that this situation occurs only in a select set of candidates. As seen from Table 2.1 $2\nu\beta\beta$ decay has been observed in only about 10 candidates out of a possible set of about 40 candidates.

Since all even-even nuclei have 0^+ ground states, the matrix element between the 0^+ ground states of the initial and final nucleus is the quantity of interest. The decay to an excited state of the final nucleus is also possible but this decay can be enormously suppressed due to the much smaller phase space available to it because of the decreased energy release in the decay. It is possible in some candidates that this matrix element to the excited state partially compensates for the decrease in phase space making this decay an important (yet easily recognizable because of the characteristic decay spectrum of the final nucleus to its ground state) background to $\beta\beta$ decay. The decays $(0_i^+ \rightarrow 0_{1f}^+)$ (where 0_{1f} is the first excited 0^+ state of the final nucleus) and $(0_i^+ \rightarrow 2_f^+)$ have been measured for several candidates.

One of the approximations used in the calculation of $M^{2\nu}$ assumes closure, *i.e.*, one replaces the energy denominator by an average value, $\bar{E}$, and performs the sum over the intermediate 1^+ states using closure and thus calculates the 2ν matrix element as, $M^{2\nu} = M_c/\bar{E}$ where

$$M_c = \langle 0_f^+ | \hat{\mathbf{G}} \cdot \hat{\mathbf{G}} | 0_i^+ \rangle. \tag{2.16}$$

The natural unit in which to measure the matrix element, $M^{2\nu}$, is obtained from the approximate sum rule for the closure matrix element [11, 12] obtained by considering the commutator $[\hat{\mathbf{G}}^\dagger \cdot \hat{\mathbf{G}}^\dagger, \hat{\mathbf{G}} \cdot \hat{\mathbf{G}}]$ in a state of isospin projection, $T_z = \frac{1}{2}(N - Z)$ as,

$$|M_c|^2 \approx 6(N - Z)(N - Z + 1). \tag{2.17}$$

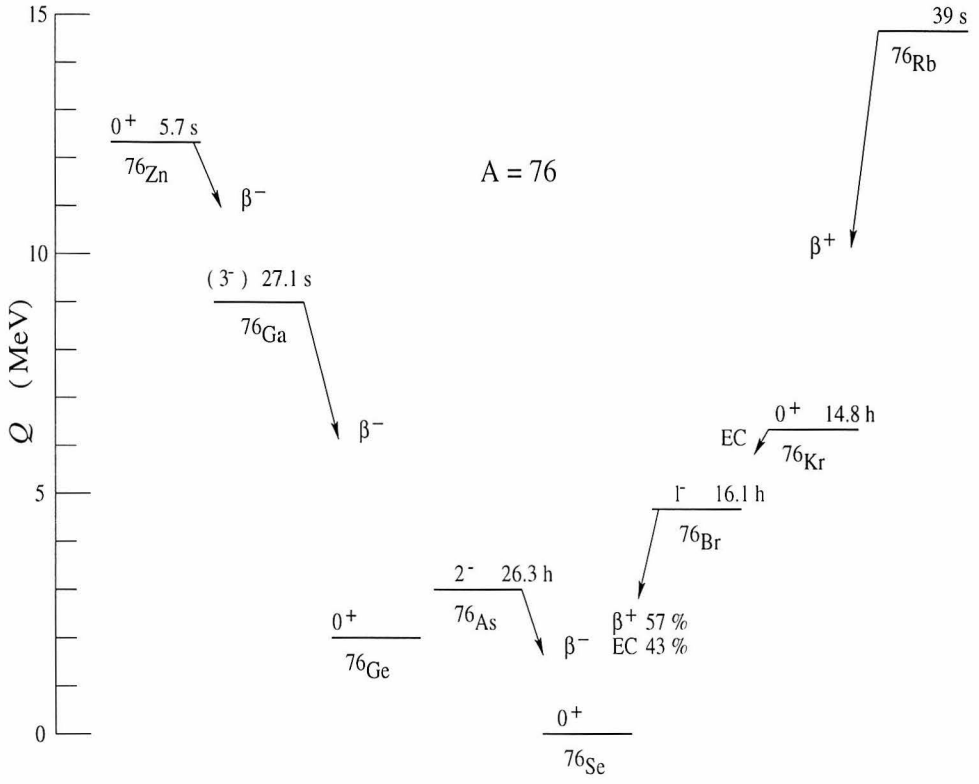

Figure 2.3: Decay scheme for $A = 76$ nuclei. The single β decays of ^{76}Ge and ^{76}Se are energetically suppressed and it is favourable for ^{76}Ge to decay to ^{76}Se through $\beta\beta$ decay.

Table 2.1: Experimentally observed β^- β^- decay candidates

Candidate	T_0 (MeV)	$T_{1/2}^{expt}$ (y)	Reference
^{48}Ca	4.27	$(5.5^{+3.5}_{-1.5}) \times 10^{19}$	[13]
^{76}Ge	2.04	$(1.43 \pm 0.03^{stat} \pm 0.13^{syst}) \times 10^{21}$	[14]
^{82}Se	2.99	$(1.08^{+0.26}_{-0.06}) \times 10^{20}$	[15]
^{96}Zr	3.35	$(3.9 \pm 0.9) \times 10^{19}$	[16]
^{100}Mo	3.03	$(1.15^{+0.30}_{-0.20}) \times 10^{19}$	[17]
^{116}Cd	2.80	$(2.6^{+0.9}_{-0.5}) \times 10^{19}$	[18]
^{128}Te	0.87	$(7.7 \pm 0.4) \times 10^{24}$	[19]
^{130}Te	2.5	$(2.7 \pm 0.1) \times 10^{21}$	[19]
^{150}Nd	3.37	$(1.7^{+1.0}_{-0.9} \pm 0.35) \times 10^{19}$	[20]
^{238}U	1.15	$(2.0 \pm 0.6) \times 10^{21}$	[21]

The correction terms to this sum rule are model dependent but generally much smaller. Thus, if one assumes an average energy denominator of order 10 MeV one obtains for $M^{2\nu} \approx \sqrt{6(N-Z)(N-Z+1)}/10$ (in units of MeV^{-1}). Experimentally, from Table 2.2, one sees that this matrix element is much smaller than that given by the sum rule. This makes a calculation of the matrix element extremely difficult as it will then depend sensitively on poor and undetermined pieces of the wavefunction.

Empirically, this smallness of $M^{2\nu}$ can be understood from the distribution of the β^- and β^+ strengths of the initial and final nucleus respectively. From Eq. (2.10) we see that the calculation of $M^{2\nu}$ is equivalent to a full description of these strength functions. The β^- strength distributes itself around 10 MeV or so in the daughter nucleus due to the repulsive nature of the spin dependent proton-neutron force in the particle-hole scheme whereas the attractive particle-particle part locates an appreciable strength of the β^+ excitation at much lower energies (see section 4.1) in the daughter. This energy mismatch results in a small overlap and hence a small $M^{2\nu}$.

For the case of ^{48}Ca, Zamick and Auerbach explained the smallness of $M^{2\nu}$ using the K-selection rule in the Nilsson pairing model [22]. In an extreme single particle picture in the Nilsson model, the 8 neutrons occupy single particle orbits of $K = 1/2, 3/2, 5/2,$ and $7/2$ (corresponding to the $f_{7/2}$ orbital). Then, $\beta\beta$ decay involves changing two neutrons from $K = 7/2$ to two protons in the $K = 1/2$ orbit which is not permitted by the GT operator as it can change K by atmost 1 unit. A shell model calculation in an $f_{7/2}^8$ configuration reveals that upon writing the ^{48}Ti ground state wavefunction as

$$|^{48}\mathrm{Ti}; 0^+\rangle = \sum_J \alpha_J |\pi f_{7/2}^2 J : \nu f_{7/2}^6 J; 0^+\rangle \tag{2.18}$$

the single beta decay amplitudes to the $J = 0$ and $J = 2$ components cancel each other to an appreciable extent. Thus, in addition to an energy mismatch in the GT distributions, strong cancellations occur resulting in a small matrix element.

Such small deviations from zero (compared to the sum rule unit) imply some symmetry. Indeed, the $SU(4)$ Hamitonian is one which gives a zero matrix element. Treating the $SU(4)$ violating parts in perturbation theory leads to the $\beta\beta$ matrix element of the correct order of magnitude [23]. However, $SU(4)$ symmetry in nuclei is known to be a crude symmetry. The spin-orbit splitting in addition to the pairing interaction is expected to be the main symmetry breaking mechanism. Investigations of the appropriateness of this symmetry in sd-shell nuclei [24] reveals that the two-body interaction is largely $SU(4)$ conserving and restores the symmetry to some extent with overlaps of the $SU(4)$ eigenstates with the ground states of various nuclei in this mass region to be only about 40%. However, there are some features in nuclei that are apparently manifestations of this symmetry or at least these features are known to occur in the $SU(4)$ limit. The occurrence of

the giant GT resonance close in energy to the Isobaric Analogue State (IAS) is one such feature. The smallness of the 2ν matrix element may be another reminiscent of $SU(4)$.

2.3 Calculational techniques for $M^{2\nu}$

2.3.1 Shell Model

The method of choice for calculating GT strengths and $M^{2\nu}$ is the nuclear shell model. This model is a microscopic approach to nuclear structure and one can, in principle, have detailed wavefunctions.

The shell model [25] is known to give an accurate and consistent description of nuclear properties in light [26, 27] and medium heavy [28] nuclei. In this model, nucleons (protons and neutrons) move in a common one-body potential (which is typically the harmonic oscillator spectrum with a strong spin-orbit force) and interact via a residual interaction which is responsible for nuclear properties like collective excitations, pairing etc. The single-particle states (shown in Fig. (2.4) are labelled by the quantum numbers $nljm$ (n is the principal quantum number corresponding to the harmonic oscillator shell, l is the orbital angular momentum, j is the angular momentum obtained from the coupling of the spin and l, and m is the z-component of j). Calculations typically involve a filled core of inert nucleons and active valence nucleons near the fermi surface in a model space that comprises a selected set of single particle states.

The two-body residual interaction between these valence nucleons is completely specified by the set of anitsymmetrized matrix elements of the form $V_{JT}(ab, cd)$ (where a, b, c, and d label the single particle orbits and J and T are the angular

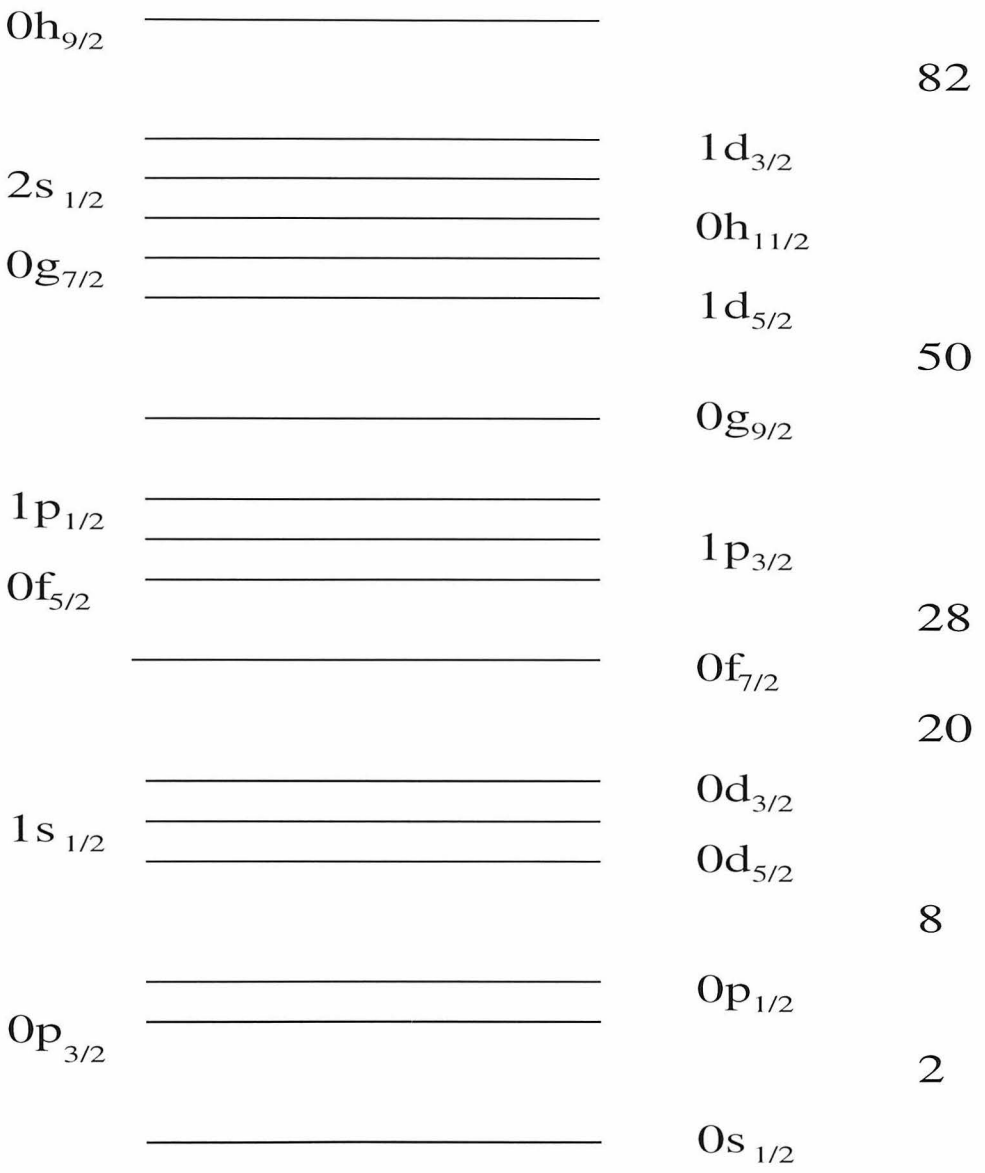

Figure 2.4: Empirical single particle spectrum used in the shell model.

momentum and isospin respectively) and can be chosen in several ways. One can vary the single-particle energies and the interaction strengths giving best-fit to a number of nuclear properties like energy levels, masses, quadrupole moments etc [26, 27]. Another philosophy is to start with the nucleon-nucleon interaction and derive an effective interaction using a G-matrix to approximate the repulsive core in the nucleon-nucleon interaction [29]. While this scheme is typically reasonable, Poves and collaborators suggest an improvement that involves changing certain monopole pieces of these interactions [30] to account for the saturation properties of nuclear matter reliably. The KB3 interaction used in this work (and several others like [28] etc.) is one such interaction.

In this model, a realistic description of the low-lying states of nuclei typically requires at least one major shell. For nuclei described in this work, the $0f1p$ shell (i.e. in the valence space of $0f_{7/2}$, $0f_{5/2}$, $1p_{3/2}$, $1p_{1/2}$ levels) would require $N_s = 20$ (where N_s is the number of single-particle states), the $(0f_{5/2}, 1p, 0g_{9/2})$ levels with $N_s = 22$ etc. The number of many-body states in this space of Z protons and N neutrons is a combinatorial factor given by $\binom{N_s}{Z}\binom{N_s}{N}$. Thus, nuclei like ^{76}Ge in the $(0f_{5/2}, 1p, 0g_{9/2})$ model space would require as many as 10^8 many-body states for an accurate description and are already beyond the scope of the traditional direct-diagonalization methods used to solve this problem.

Thus, the exponential explosion of the many-body space prevents realistic calculations in heavier nuclei. Complete $0\hbar\omega$ calculations of $M^{2\nu}$ via direct-diagonalization have been possible for the lightest of $\beta\beta$ candidates, ^{48}Ca. More recently, heavier nuclei such as ^{82}Se have been investigated in complete model spaces using direct-diagonalization [31].

The Gamow-Teller operator connects only spin-orbit partners in the single-particle picture. Thus, a β^+ transition for the lower mass nuclei in the pf-shell

(shown in Fig. 2.5 for ^{48}Ti) involves changing a proton in $f_{7/2}$ to a neutron in $f_{7/2}$ or $f_{5/2}$. Two-neutrino double beta decay involves a sequence of such GT transitions. Since, for the nuclei considered, the $f_{7/2}$ is at least nearly full in neutrons, the $\pi f_{7/2} \rightarrow \nu f_{7/2}$ transition is Fermi-blocked resulting in a significant suppression of $B(GT_+)$. In addition, this strength is suppressed by spin-isospin neutron-proton correlations, e.g., Ref. [32]. In any calculation that includes all the spin-orbit partners, the β^- transition (which involves changing a neutron in the $f_{7/2}$ to a proton in either of the spin-orbit partners) and the β^+ transition participate in a model-independent Ikeda sum rule given by $B(GT_-) - B(GT_+) = 3(N - Z)$.

The 2ν matrix element can be written as $M^{2\nu} = \sqrt{B(GT_+)B(GT_-)}\ \sum_m\ C_m$ (where $B(GT_+)$ is the β^+ strength of the daughter nucleus and $B(GT_-)$ is the β^- strength of the parent and C_m provides the remaining contribution to the sum in $M^{2\nu}$) and thus some role in the suppression of $M^{2\nu}$ is played by the $B(GT_+)$ suppression.

In their pioneering work Haxton and Stephenson used a truncation scheme based on the weak coupling approximation and evaluated $M^{2\nu}$ assuming closure. In this scheme they obtained separate proton (neutron) wavefunctions for four, six and eight valence particles (two, four, six and eight valence holes) in the $(1p_{1/2}, 1p_{3/2}, 0f_{5/2}, 0g_{9/2})$ model space. Then, the fifty lowest proton and neutron states were combined to form a basis which were then allowed to mix through the proton-neutron interaction and the resulting matrix was diagonalized to obtain the wavefunctions and eigenvalues. Even though the truncations in this scheme are severe, this procedure was generally expected to account for the low-lying states reasonably well.

However, performing the sum in $M^{2\nu}$ assuming closure is now known not to be a very good approximation for calculating the matrix element. One could, of

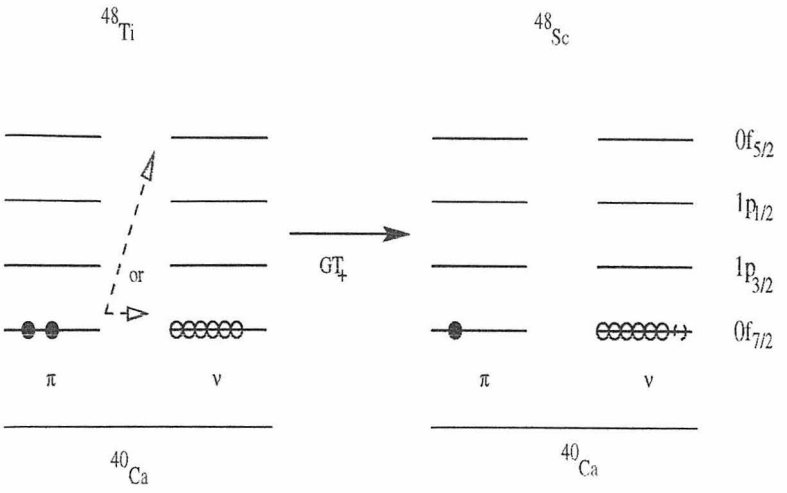

Figure 2.5: β^+ transition mediated by the GT_+ operator (shown for ^{48}Ti in the pf-shell above a ^{40}Ca core) in the extreme single-particle picture in the shell model. In this transition a proton in the $f_{7/2}$ can change into a neutron in either the $f_{7/2}$ or the $f_{5/2}$. Note that the transition to $f_{7/2}$ is significantly blocked due to the Pauli principle.

course, consider closure to be a definition of $\bar{E}$, the average energy denominator, and thus consider the validity of the closure approximation as a question of choice of $\bar{E}$. However, since one is then expected to know $M^{2\nu}$ to calculate $\bar{E}$, the prescription for choosing $\bar{E}$ is not very clear. In addition, if there are significant cancellations in the matrix element this approximation could fail badly. Haxton *et al.* chose the position of the β^- giant GT resonance for $\bar{E}$. This, of course, is not the obvious choice as one could also have chosen the centroid of the β^+ strength for the final nucleus or even an average of the two energies for the average energy denominator.

More recently, truncated calculations for heavier nuclei using the shell model have become available [31].

Table 2.2 shows all the known experimental and calculated $M^{2\nu}$ for several 2ν

Table 2.2: Matrix elements (in units of MeV^{-1}) for the various observed $\beta\beta$ candidates. The experimental results using half-lives from Table 2.1 are also shown (with $g_A = 1.0$ in the phase space factor). A "-" indicates that there are no calculations for $M^{2\nu}$.

Candidate	$M^{2\nu}_{expt}$	$M^{2\nu}_{QRPA}$	$M^{2\nu}_{SM}$
^{48}Ca	≈ 0.065	0.041 [33]	0.08[34]
^{76}Ge	0.221	0.24[35]	0.14[31]
^{82}Se	0.146	0.14[35]	0.164[31]
^{96}Zr	0.104	0.24[35]	-
^{100}Mo	0.326	0.24[35]	-
^{116}Cd	0.220	-	-
^{128}Te	0.039	0.14[35]	0.244[9]
^{130}Te	0.027	0.098[35]	0.232[9]
^{150}Nd	0.070	-	-
^{238}U	0.086	-	-

candidates. A "-" is shown where no calculation exists. We now discuss the shell model entries in Table 2.2 (column 4).

The ^{48}Ca calculation indicated is performed in the complete $(0f, 1p)$ shell [34]. Further discussions of other calculations and the comparison of these results with experiment are given in section 4.2.3. The results for ^{76}Ge are obtained from a calculation in the $(1p, 0f_{5/2}, 0g_{9/2})$ single-particle space with utmost four particles allowed into the $g_{9/2}$ from the lower $(f_{5/2}, p)$ space [31]. This is the same space as the Haxton calculation but involves a less severe truncation. However, the effect of this truncation is uncertain. Naively, one might expect that an untruncated calculation in this model space might have additional β^+ strength due to the extra neutron holes introduced in the $(f_{5/2}, p)$ space due to the unrestricted smearing of the neutron fermi surface. The ^{82}Se matrix element is obtained from an unrestricted calculation in the same model space [31]. Other shell model results in

the table are from the calculation of the closure matrix element by Haxton *et al.* mentioned previously.

The decay of ^{100}Mo $\rightarrow$ ^{100}Tc $\rightarrow$ ^{100}As can prove to be a good test of theory. In this case the intermediate nucleus has a ground state that happens to be 1^+ and can decay to the ground states of the initial and final nucleus by electron capture and β^- decay respectively. Both the electron capture and the β^- $\log ft_{1/2}$ value are known experimentally [36]. This known 1^+ state by itself essentially gives the correct value of the matrix element. Thus, in an appropriate calculation the matrix element under the closure approximation should give the same answer as the full matrix element. The same curious phenomenon occurs in the case of ^{128}Te $\rightarrow$ ^{128}I $\rightarrow$ ^{128}Xe, where the ground state of ^{128}I (which happens to be 1^+) carries most of the 2ν strength.

The nuclear matrix elements obtained from the closure approximation for ^{128}Te and ^{130}Te are in sharp disagreement with those from experiment. From a comparison of the average energy denominator used in the weak coupling approximation with that obtained from direct-diagonalization calculation in ^{48}Ca (7.20 MeV versus 3.3 MeV) one can see that this choice of $\bar{E}$ is significantly overestimated in the former. Thus, while this disagreement with the experimental $M^{2\nu}$ in the Te nuclei might point to a failure of the weak coupling approximation, it is also true that these matrix elements are even more suppressed relative to matrix elements of other nuclei making them more difficult to calculate.

2.3.2 Quasi-Particle Random Phase Approximation

The quasi-particle random phase approximation (QRPA) has been used to study various excitation modes in even-even nuclei. The calculation of β decay rates

through the matrix elements of the GT operator has been an important application.

Most recent calculations of $M^{2\nu}$ for nuclei heavier than ^{48}Ca use the QRPA methods. This approach is computationally simple and includes many features of the two-body interaction known to be relevant for β and $\beta\beta$ decay. In this method, the proton-proton and neutron-neutron particle-particle interactions are included using the BCS quasiparticle scheme. Besides the smearing of the Fermi surface introduced by the pairing interaction in the BCS scheme, the spin dependent neutron-proton interaction is another important ingredient that is included in these calculations.

QRPA is a theory of small amplitudes of collective motion. While this theory accounts for the small value of $M^{2\nu}$, it has low predictive power. Engel *et al.* [35] found an extreme sensitivity of the total strength in the β^+ direction, $B(GT_+)$, of the final nucleus and hence $M^{2\nu}$ to the particle-particle force, g_{pp}, in the $J = 1$, $T = 0$ channel and their prescription was to fix the value of the strength in this channel by comparing the $B(GT_+)$ of several nuclei to known experimental values. The 2ν matrix elements were found to vanish near this realistic value of g_{pp} ($g_{pp} \approx 1$) making the actual value of $M^{2\nu}$ very uncertain. Shown in column 3 of Table 2.2 are the $M^{2\nu}$ obtained from QRPA calculations. While the matrix elements are in reasonable agreement with experiment for several nuclei, they are significantly overestimated for ^{96}Zr and the Te nuclei. Being deformed nuclei, a reliable description of ^{150}Nd and ^{238}U requires the use of a deformed basis such as the Nilsson wavefunctions. Such a task within the QRPA is still an outstanding one.

We now return to the question of the crossing of zero for $M^{2\nu}$ in QRPA. In the region of the relevant g_{pp} one finds that the amplitudes become large and the

required matrix element needs to be calculated very close to a phase transition. Recently, a new scheme, the so-called renormalized QRPA [37], has been introduced that seeks to move this instability away from a realistic value of g_{pp} by including higher order terms in QRPA. As QRPA calculations take place near a phase transition where fluctuations are non-trivial, whether such an approach of including more terms in a harmoni expansion is a reliable tool to calculate $M^{2\nu}$ remains to be seen.

The question that naturally arises is whether this crossing of zero of $M^{2\nu}$ is an artifact of QRPA or a physical effect. If the latter were the case, such an effect should be seen even in the shell model near the physical Hamiltonian. The QRPA and shell model have been compared in several studies [38, 33]. Fig. 2.6 shows the square of the matrix element and the total β^+ strength, $B(GT_+)$, of ^{48}Ti versus this parameter g_{PP} obtained by us from a direct-diagonalization calculation for the decay of ^{48}Ca (see Chapter 4). The overall phase of the matrix element is indeterminate in such a calculation and only the square of this quantity enters the physically meaningful half life. (Direct-diagonalization calculations being "exact" have no errors associated with them.) In the absence of the $J = 1, T = 0$ channel ($g_{PP} = 0$) both quantities are relatively unsuppressed. The 2ν matrix element tracks the $B(GT_+)$ generally. The square of the 2ν matrix element has a minimum very close to zero (as in QRPA models). However, as we shall see in section 4.2.3 this minimum is disallowed by the interaction as at this value of g_{PP} agreement with experiment in other quantities is destroyed. Nevertheless, this sensitivity to the 1^+ interaction in two different solutions to the many-body problem indicates that the mechanism for the suppression of $B(GT_+)$ and $M^{2\nu}$ arises in the enhancement of the spin-isospin correlations in the ground state which are dominantly affected by the $J = 1, T = 0$ channel in the two-body interaction.

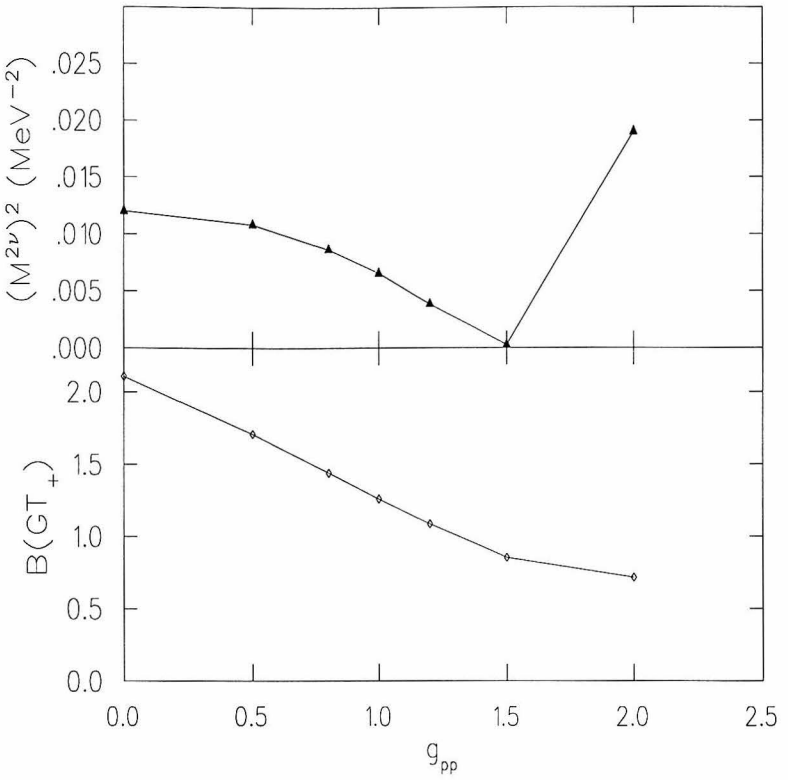

Figure 2.6: The upper panel shows the square of $M^{2\nu}$ versus the strength of the particle-particle interaction in the $J = 1, T = 0$ channel, g_{PP}, from the shell model for the decay of ^{48}Ca. The lower panel shows $B(GT_+)$ for ^{48}Ti versus g_{PP}.

A number of other QRPA calculations have been performed by several other groups. See Ref [39] and [40] for a review.

2.4 GT operator and g_A quenching

Theoretical models thought to be appropriate overestimate the observed GT_+ and GT_- strengths in nuclei. Shell model calculations generally recover more suppression of these strengths than QRPA calculations do. However, calculations

in complete $0\hbar\omega$ spaces using the shell model require approximately an overall renormalization for agreement with experiment in the case of both individual transitions between well defined nuclear states in the sd [41] and pf [42] shell and for the total GT strengths. The experimental distributions are described reasonably well in the shell model with the appropriate strengths at appropriate energies apart from this overall renormalization.

The experimental distributions are obtained from the intermediate-energy charge exchange (n,p) or (p,n) cross sections at low momentum transfers. For such forward angle reactions, the $L = 0$ transitions dominate and so the (n,p) and (p,n) reaction should excite transitions analogous to the β^+ and β^- decay between the same states. This proportionality between the cross section and the GT strength allows one to obtain the strength distribution. However, for energies higher than about ~ 8 MeV, higher multipole components and other effects that produce a neutron begin to dominate the cross section making it difficult to reliably extract the GT strength (see section 3.2 for a discussion of the of ^{48}Ti case).

A number of explanations have been proposed for this observed "quenching" of the GT strengths. One of these invokes sub-nucleonic degrees of freedom and excites Δ resonances through the GT operator in the constituent quark model thereby pushing some strength out to about 300 MeV [43, 44]; unobservable in (n,p) or (p,n) reactions. Another explanation relies on the renormalization of the axial-vector coupling constant to $g_A = 1$ in the nuclear medium. A third explanation simply is that configuration mixing effects from high-lying states are ignored in such shell model calculations and thus one may need to use an effective spin operator to account for missing correlations.

Thus, two facts are clear: a) Shell model calculations recover the GT strength

distributions but not the overall strengths. A simple renormalization of the spin operator by a factor of $\sim 1/(1.26)^2$ brings the strengths into better agreement with experiment. b) Some strength at higher energies being buried in high backgrounds may evade detection in experiments and so the experimental total strength must be considered as a lower limit.

We note that for the 2ν decay g_A appears in the fourth power (Eq. (2.9)). If the quenching of g_A is the solution, this amounts to an increase of the calculated half-life by almost a factor of three. However, due to uncertainties in the calculation, for instance, the choice of the interaction, it is not very clear that all transition matrix elements require the same renormalization [42]. Since the 2ν matrix element involves a summation over *all* intermediate 1^+ states, it is not *a priori* clear that this prescription of overall renormalization is applicable to 2ν decay. As we shall see in section 4.2.3, theoretical calculations cannot be constrained well enough to resolve this issue. In this work, we will use bare $\boldsymbol{\sigma}\tau$ operators for the 2ν decay unless specified otherwise.

2.5 Experimental Techniques

Attempts to directly observe $\beta\beta$ decay were unsuccessful for nearly four decades. With half lives of the order of 10^{20} years, this process needs to be detected in experiments with extremely low backgrounds. In addition, the $2\nu\beta\beta$ decay has an experimental signature in the form of a continuous sum energy spectrum of the emitted electrons making it more difficult to distinguish from the background.

Measurements involve three different techniques as briefly described below:

1) Geochemical determinations: In such experiments one determines the excess of the daughter isotope that has accumulated over geologic times in a natural

mineral of the parent element. The signature for the production of the daughter isotope is an increase in its isotopic abundance relative to some reference isotope of the same element not produced in $\beta\beta$ decay. These determinations can be made in cases where the daughter nucleus is a noble gas though recently, an attempt has been made to study the decay: ^{96}Zr $\rightarrow$ ^{96}Mo [16]. Noble gases are minor components in the earth's crust and so isotopic excesses due to $\beta\beta$ decays can be measured if accumulated over geologic times and if independent calibrations exist for determining the gas retention properties of the ore.

The first evidence for $\beta\beta$ decay was found for the decay of ^{130}Te [45] and this result was later confirmed by several independent experiments (see Ref. [46] for the latest review). Since then this technique has been applied successfully to other known $\beta\beta$ decay candidates whose daughters are noble gases viz. ^{82}Se $\rightarrow$ ^{82}Kr, ^{128}Te $\rightarrow$ ^{128}Xe.

Early experiments on ^{128}Te did not provide a good constraint on $\beta\beta$ decay of this isotope as it has a low energy release for this decay (T_0 = 0.869 MeV) and thus has an exceptionally long half life. It was only recently that a half life that took into account calibration uncertainties of $T_{1/2} = (7.7 \pm 0.4) \times 10^{24}$ was measured [19].

Since gas retention ages of minerals are not very well known, absolute values of individual half lives measured by the geochemical method are subject to unquantifiable errors. By measuring the ratios of half lives of similar isotopes like ^{130}Te and ^{128}Te this question of gas loss can be circumvented. Also, the low Q-value for ^{128}Te suppresses 2ν relative to other modes and thus as suggested by Pontecorvo [47] the ratio of half lives may provide a sensitive test for the existence of 0ν decay.

^{82}Se is the only nucleus whose half life for the 2ν decay has been measured

by both geochemical methods and direct detection (see section 3). Both yield consistent half lives of $T_{1/2} = 1.0 \times 10^{20}$ years.

2) Radiochemical experiments

Total rates can also be measured in radiochemical experiments. In these experiments, a given volume of the parent nucleus accumulates a sufficient number of daughter nuclei which are then extracted chemically and counted. This technique is possible if the daughter isotope is radioactive (with a half life much smaller than geologic times) and thus countable by standard techniques. As in geochemical experiments, there is no information of the $\beta\beta$ decay spectrum of emitted electrons. This technique was used successfully for the first time recently, where a half life for the decay ^{238}U $\rightarrow$ ^{238}Pu was reported [21]. ^{238}Pu has a half life of ~ 90 years and decays by emission of a ~ 5 MeV α particle. ^{238}U is another candidate with a low Q-value ($Q = 1.15$ MeV) and therefore is a good candidate for detection of 0ν decay.

3) Direct-counting experiments

In these experiments the single electron spectra, the summed-electron spectra and the opening angle of the emitted electrons can be recorded. $2\nu\beta\beta$ decay was first directly observed in 1987 [2] using a thin film of ^{82}Se as the source in a Time Projection Chamber (TPC). The emitted electrons ionize the He gas in the TPC and the ionization electrons drift towards the ends of the chamber where a grid of wires records their arrival. The tracks of the primary electrons emitted in $\beta\beta$ decay are then reconstructed. A positive identification of $2\nu\beta\beta$ was made with $T_{1/2} \simeq 1.1 \times 10^{21}$ years.

^{76}Ge is one of the few other nuclei where the $2\nu\beta\beta$ decay has been precisely measured and the best limits on the 0ν decay have been obtained. This decay has small energy release ($Q = 2.045$ MeV) compared to many other candidates,

making this decay relatively unfavoured. However, this is offset by the fact that semiconductor ^{76}Ge is very pure and contains almost no radioactivity except for cosmogenic activity which decays once underground. The worst impurity, ^{68}Ge, has a half life of 288 days. Isotopically enriched ^{76}Ge is then used both as a source and as a high resolution ($\approx$ 3 KeV) calorimetric detector. The Heidelberg-Moscow group have 12 kg of germanium enriched to 86% in ^{76}Ge in the form of five crystals, three of which are operating in Gran Sasso. They obtain a half life of 2ν decay as $T_{1/2} = 1.42 \times 10^{21}$ years and a limit on the 0ν decay as $T^{0\nu}_{1/2} > 1.6 \times 10^{24}$ years at 90% c.l. [14], the strictest limit on 0ν decay so far.

Other direct-detection experiments online to detect $\beta\beta$ decay include that on ^{136}Xe [48]. The TPC is filled with ^{136}Xe gas thus providing information on both the total energy (measured calorimetrically) and tracks of the emitted electrons.

A more detailed discussion of the experimental status regarding direct-detection of $\beta\beta$ decay is given in Ref. [49]

Chapter 3 Numerical Methods

In this chapter, numerical techniques involved in the Shell Model Monte Carlo is reviewed. The discussion includes a practical solution to the "sign problem" that is employed in obtaining observables for realistic interactions. A Maximum Entropy method to extract strength functions from response functions is also discussed. Finally, the function from which one can calculate the 2ν matrix element is presented and the computational aspects involved in such a calculation is discussed.

The Shell Model Monte Carlo (SMMC) scales more gently with the number of valence nucleons and valence orbits than traditional methods used to solve the shell model as it does not explicitly enumerate the various many-body states and thus is a powerful tool to study heavier nuclei. Detailed descriptions of the SMMC can be found in the literature [50, 51] and so only a brief description is attempted here.

SMMC methods are well suited to calculating thermal averages of observables. These methods exploit the fact that most of the billions of configurations in nuclei are quite unimportant for general nuclear properties and so only a subset of the relevant configurations need be sampled. Although properties of a specific state cannot be calculated we can obtain ground state properties by going to low temperatures. This precludes detailed spectroscopic information; however, as we shall see, we can obtain information about the spectrum through response functions. In addition, the expectation value of one and two body operators can yield interesting information about the nuclear system. The double beta decay calculation

requires a four body operator.

3.1 The Shell Model Monte Carlo

The SMMC method is based on a statistical formulation. The canonical expectation value of an operator $\hat{\mathcal{A}}$ at a given temperature T is given by [52, 50, 53, 54, 51] ($\beta = 1/T$)

$$\langle \hat{\mathcal{A}} \rangle = \frac{\mathrm{Tr_A}[\hat{\mathcal{A}} e^{-\beta \hat{H}}]}{\mathrm{Tr_A}[e^{-\beta \hat{H}}]}, \tag{3.1}$$

where $\hat{U} = \exp(-\beta \hat{H})$ is the imaginary-time many-body propagator and $\mathrm{Tr_A}\hat{U}$ is the canonical partition function for A nucleons. The shell model Hamiltonian, $\hat{H}$, has utmost two-body interactions and can be cast in the form

$$\hat{H} = \sum_{\alpha} \left(\epsilon_{\alpha}^{*} \bar{\mathcal{O}}_{\alpha} + \epsilon_{\alpha} \mathcal{O}_{\alpha} \right) + \frac{1}{2} \sum_{\alpha} V_{\alpha} \left\{ \mathcal{O}_{\alpha}, \bar{\mathcal{O}}_{\alpha} \right\} , \tag{3.2}$$

where ϵ_{α} are the single particle energies and $\mathcal{O}_{\alpha}$ represent a set of one-body density operators ($\bar{\mathcal{O}}$ denotes the time-reversed partner of $\mathcal{O}$). The Hamiltonian in Eq. (3.2) is manifestly time-reversal invariant if the parameters V_{α} that define the strength of the residual two-body interactions are real.

To obtain the V_{α} from the residual particle-particle interaction, $V_{JT}(ab, cd)$, requires a Pandya transformation whose details are given in [50].

The two-body operators in $\hat{H}$, in principle, connect one Slater determinant to all other Slater determinants and thus one has to keep track of a large number of Slater determinants and diagonalise $\hat{H}$ in the space of all many-body states making this problem a computational challenge. The key to the SMMC method is to rewrite the propagator $\hat{U}$ as a functional integral over one-body propagators.

To this end, the exponent in $\hat{U}$ is split into N_t time slices of duration $\Delta\beta = \beta/N_t$,

$$\hat{U} = \left[e^{-\Delta\beta\hat{H}}\right]^{N_t}. \tag{3.3}$$

The many-body propagator at each time slice is linearized by a Hubbard-Stratonovich (HS) transformation [55, 56]; *i.e.*, it is transformed into an integral over a set of one-body propagators that correspond to non-interacting nucleons in fluctuating auxiliary fields defined by complex c-numbers $\sigma_{\alpha n}$ $(n = 1, ..., N_t)$ yielding for $\hat{U}$

$$\hat{U} = \left[\exp\left(-\Delta\beta\hat{H}\right)\right]^{N_t} \simeq \int D[\sigma]G(\sigma)\hat{U}_\sigma \tag{3.4}$$

where the integration measure is

$$D[\sigma] = \Pi_{\alpha n}[d\sigma_{\alpha n}d\sigma^*_{\alpha n}\Delta\beta|V_\alpha|/2\pi], \tag{3.5}$$

the Gaussian factor is

$$G(\sigma) = \exp(-\frac{1}{2}\sum_{\alpha n}|V_\alpha\|\sigma_{\alpha n}|^2\Delta\beta), \tag{3.6}$$

the one-body propagator is

$$\hat{U}_\sigma(\beta, 0) \equiv \hat{U}_\sigma = \hat{U}_{N_t}\cdots\hat{U}_1 \tag{3.7}$$

with $\hat{U}_n \equiv \exp[-\Delta\beta\hat{h}_n]$, and the one-body Hamiltonian for the n^{th} time slice is

$$\hat{h}_n = \sum_\alpha(\epsilon^*_\alpha + s_\alpha V_\alpha\sigma_{\alpha n})\bar{\mathcal{O}}_\alpha + (\epsilon_\alpha + s_\alpha V_\alpha\sigma^*_{\alpha n})\mathcal{O}_\alpha, \tag{3.8}$$

with $s_\alpha = \pm 1$ for $V_\alpha < 0$ and $s_\alpha = \pm i$ for $V_\alpha > 0$. The commutator terms from

the operators in $\hat{H}$ render the HS transformation accurate through order $\Delta\beta$ and thus this approximation becomes exact as $N_t \to \infty$ or $\Delta\beta \to 0$.

The expectation value of $\hat{\mathcal{A}}$ is then calculated through

$$\langle \hat{\mathcal{A}} \rangle_A = \frac{\mathrm{Tr_A}[\hat{\mathcal{A}} e^{-\beta \hat{H}}]}{\mathrm{Tr_A}[e^{-\beta \hat{H}}]} \approx \frac{\int D[\sigma] W(\sigma) \Phi(\sigma) \langle \hat{\mathcal{A}} \rangle_\sigma}{\int D[\sigma] W(\sigma) \Phi(\sigma)}. \tag{3.9}$$

The non-negative weight is

$$W(\sigma) = |Z_A(\sigma)| G(\sigma) \tag{3.10}$$

where $Z_A(\sigma) = \mathrm{Tr_A} \hat{U}_\sigma$ is the canonical trace (with fixed number of nucleons, A). The "sign" is $\Phi(\sigma) = Z_A(\sigma)/|Z_A(\sigma)|$ and the expectation value of $\hat{\mathcal{A}}$ with respect to the auxiliary field σ is

$$\langle \hat{\mathcal{A}} \rangle_\sigma = \mathrm{Tr_A}[\hat{\mathcal{A}} \hat{U}_\sigma] / Z_A(\sigma). \tag{3.11}$$

Since $\hat{h}_n(\sigma)$ is only a one-body operator, the evolution operator $\hat{U}(\sigma)$ can be represented as a $N_s \times N_s$ matrix $\mathbf{U}_\sigma$ in the single-particle basis. and both $Z_A(\sigma)$ and $\langle \hat{\mathcal{A}} \rangle_\sigma$ can be evaluated in terms of the matrix $\mathbf{U}_\sigma$.

The computational effort scales as $(N_s)^3 \cdot N_t$ (from the N_t matrix multiplications of the $N_s \times N_s$ matrices, $\mathbf{U}_\sigma$). The dimension of the integral in Eq. (3.9) scales as $(N_s)^2 N_t$ and is independent of the number of nucleons in the valence space. For instance, this number for pf-shell nuclei is $\sim 10^5$. This multi-dimensional integral can be evaluated by Monte Carlo methods using samples generated by the algorithm of Metropolis *et al.* [57] as described in Ref. [58, 50, 51]. Thus, the

expectation value of $\hat{\mathcal{A}}$ is calculated as

$$\langle \hat{\mathcal{A}} \rangle = \frac{\frac{1}{N}\sum_i \langle \hat{\mathcal{A}} \rangle_i \phi_i}{\frac{1}{N}\sum_i \phi_i} \tag{3.12}$$

where N is the number of Monte Carlo samples.

However, because of the large number of auxiliary fields involved, successive field configurations are highly correlated for a reasonable acceptance (~ 0.5), the autocorrelation being over 200 sweeps. To generate uncorrelated samples more efficiently, the continuous integral over each $\sigma_{\alpha n}$ has been approximated by a discrete sum derived from Gaussian quadrature. The relation

$$e^{\Delta\beta V \mathcal{O}^2/2} \approx \int_{-\infty}^{\infty} f(\sigma) e^{\Delta\beta V \sigma \mathcal{O}} \tag{3.13}$$

is satisfied through terms in $(\Delta\beta)^2$ if $f(\sigma) = \frac{1}{6}[\delta(\sigma - \sigma_0) + \delta(\sigma + \sigma_0) + 4\delta(\sigma)]$, where $\sigma_0 = (3/V\Delta\beta)^{1/2}$ and is used instead of the continuous HS transformation. In this way, each $\sigma_{\alpha n}$ becomes a 3-state variable and the path integral becomes a path sum which can be samples using the algorithm of Metropolis *et al.* This discretization in the fields reduces the correlation length to about 5 sweeps with no loss of accuracy.

Since the Hamiltonian is written as a quadratic power in the density operators $\mathcal{O}$ (and $\bar{\mathcal{O}}$) $\hat{h}_n$ can be constructed from operators that act on protons and neutrons separately leading to separate traces, *i.e.*, $Z_A(\sigma) = Z_Z(\sigma) Z_N(\sigma)$. Thus, the HS transformation does not mix protons and neutrons and their numbers will be conserved separately in each Monte Carlo sample.

In what follows the technique for projecting out the partition function for A particles from the grand canonical many-body trace [54, 51] is described. Since,

protons and neutrons do not mix what follows is valid for each type of particle and thus A in the following can mean either Z protons or N neutrons each in N_s single-particle states. Expressions for one and two body densities are also listed.

For a chemical potential μ the grand canonical trace is given by

$$\mathrm{Tr}[e^{\beta\mu\hat{N}}\hat{U}_\sigma] = \det[\mathbf{1} + e^{\beta\mu}\mathbf{U}_\sigma]. \tag{3.14}$$

One can obtain the canonical trace, Z_A, from the grand canonical trace by using the projection operator, $\hat{P}_A = \delta_{AN}$ i.e.

$$\mathrm{Tr}_A[\hat{U}_\sigma] = \mathrm{Tr}[\hat{P}_A\hat{U}_\sigma]. \tag{3.15}$$

Now, using the following identity valid for discrete A

$$\delta_{AN} = e^{-\beta\mu A}\frac{1}{N_s}\sum_{m=1}^{N_s} e^{-i\phi_m(A-N)}e^{\beta\mu N} \tag{3.16}$$

one can write Z_A as

$$\begin{aligned} Z_A &= \frac{1}{N_s}\sum_{m=1}^{N_s} e^{-i\phi_m A}e^{-\beta\mu A}\mathrm{Tr}[e^{\beta\mu N}e^{i\phi_m N}\hat{U}_\sigma] \\ &= \frac{1}{N_s}\sum_{m=1}^{N_s} e^{-i\phi_m A}e^{-\beta\mu A}\det[\mathbf{1} + e^{\beta\mu}e^{i\phi_m}\mathbf{U}_\sigma]. \end{aligned} \tag{3.17}$$

The parameter μ is arbitrary however there is a favoured choice for which this projection is numerically stable. Since Z_A vary rapidly with A a good choice for μ is one for which the terms in the sum favour $N = A$. To obtain this value of μ, we first find the N_s eigenvalues λ_i for $\mathbf{U}_\sigma$. Then defining $e^{-\beta\mu} = |\lambda_A\lambda_{A+1}|^{1/2}$ allows us to obtain the optimal value of μ.

The calculation of Z_A in Eq. (3.17) is an $(N_s)^4$ process and needs to be calculated for every Monte Carlo step which makes it a formidable task. In practice, the computation is simplified by using the eigenvalues, λ_i of $\mathbf{U}_\sigma$ in the expression for Z_A. Defining

$$\begin{aligned} \eta_m(\sigma) &= \det[\mathbf{1} + e^{i\phi_m} e^{\beta\mu} \mathbf{U}_\sigma] \\ &= \prod_{i=1}^{N_s} (1 + e^{-i\phi_m} e^{-\beta\mu} \lambda_i) \end{aligned} \tag{3.18}$$

one can write Z_A as

$$Z_A = \frac{1}{N_s} \sum_{m=1}^{N_s} e^{-i\phi_m A} e^{-\beta\mu A} \eta_m(\sigma). \tag{3.19}$$

The one and two body densities can be projected out in a similar fashion:

$$\langle a_\alpha^\dagger a_\beta \rangle = \frac{1}{N_s Z_A(\sigma)} \sum_{m=1}^{N_s} e^{-iA\phi_m} e^{-\beta\mu A} \eta_m(\sigma) \gamma_{\alpha\beta}^m(\sigma), \tag{3.20}$$

and

$$\begin{aligned} \langle a_\alpha^\dagger a_\beta a_\gamma^\dagger a_\delta \rangle &= \frac{1}{N_s Z_A(\sigma)} \sum_{m=1}^{N_s} e^{-i\phi_m A} e^{-\beta\mu A} \eta_m(\sigma) \\ &\quad \times [\gamma_{\alpha\beta}^m(\sigma) \gamma_{\gamma\delta}^m(\sigma) - \gamma_{\alpha\delta}^m(\sigma) \gamma_{\gamma\beta}^m(\sigma) + \delta_{\beta\gamma} \gamma_{\alpha\delta}^m(\sigma)] \end{aligned} \tag{3.21}$$

where $\gamma_{\alpha\beta}(\sigma)$ is defined as

$$\gamma_{\alpha\beta}(\sigma) = [(\mathbf{1} + e^{i\phi_m} e^{\beta\mu} \mathbf{U}_\sigma)^{-1} e^{i\phi_m} e^{\beta\mu} \mathbf{U}_\sigma]_{\beta\alpha}. \tag{3.22}$$

Once again, $\gamma_{\alpha\beta}(\sigma)$ is evaluated in terms of the eigenvalues λ_i and the transfor-

mation matrix, $\mathbf{T}$, associated with the diagonalization of $\mathbf{U}_\sigma$ as

$$\gamma_{\alpha\beta}(\sigma) = \sum_i \mathbf{T}_{\beta i}(1 + e^{i\phi_m} e^{\beta\mu}\lambda_i)^{-1} e^{i\phi_m} {\mathbf{T}_{i\alpha}}^{-1}. \tag{3.23}$$

3.1.1 Sign problem and a practical solution

If all $V_\alpha < 0$, then the sign is $\langle\Phi\rangle = 1$. However, for realistic nuclear interactions, several of the V_α's are positive generating a sign problem (where the uncertainty in Φ is larger than $\langle\Phi\rangle$). To circumvent this "sign problem" one first identifies the "good" and "bad" pieces of the Hamiltonian (H_G and H_B respectively) as,

$$\begin{aligned} \hat{H}_G &= \sum_\alpha \left(\epsilon_\alpha^* \bar{\mathcal{O}}_\alpha + \epsilon_\alpha \mathcal{O}_\alpha\right) + \frac{1}{2}\sum_{V_\alpha<0} V_\alpha \left\{\mathcal{O}_\alpha, \bar{\mathcal{O}}_\alpha\right\} \\ \hat{H}_B &= \frac{1}{2}\sum_{V_\alpha>0} V_\alpha \left\{\mathcal{O}_\alpha, \bar{\mathcal{O}}_\alpha\right\}. \end{aligned} \tag{3.24}$$

This decomposition of H into "good" and "bad" pieces is performed in the particle-hole channel (or rather when H is written as a quadratic in density operators) and is shown in Fig. (3.1) in the uppermost panel for the KB3 interaction. We see that about half the V_α are of bad sign but the largest V_α in magnitude are of good sign. The corresponding particle-particle interaction matrix elements for a selected set of interaction channels are shown in the lower panels in Fig. (3.1). The largest difference between the physical Hamiltonian (solid circles) and the "good" Hamiltonian, H_G, (open circles) occurs in the $J = 0, T = 1$ pairing channel.

One then defines a set of Hamiltonians $H_g = H_G + gH_B$ such that $H_{g=1} = H$ is the physical Hamiltonian. For $g \leq 0$, H_g is free of the sign problem and calculated observables are extrapolated to $g = 1$ [59]. We choose polynomial extrapolations from negative g to $g = 1$, the degree of the polynomial chosen to be the smallest

that yields a χ^2 per degree of freedom less than 1. This procedure has been shown to give accurate results (within the stated uncertainties) for the many observables for which it has been tested by comparison to direct diagonalization results in the sd and lower pf shells for ground state properties.

Note that scaling H_G as $\left(1 - \frac{1-g}{\chi}\right) H_G$, together with a g-dependent compression of the single-particle spectrum (with the value of χ chosen to make the g-extrapolation as smooth as possible) is also permitted. As before, the original Hamiltonian is recovered for $g = 1$. The introduction of this additional parameter, χ, provides a control on the g-extrapolation. A necessary condition that the calculation must satisfy is that extrapolations from calculations using different values of χ must give consistent results. This latter modification of the Hamiltonian (i.e. a finite value of χ) has been used for finite temperature studies [60].

One of the various changes in the interaction in going from the physical $g = 1.0$ case to the negative g values is that the $\chi = \infty$ family of Hamiltonians (corresponding to no scaling of H_G) makes the pairing interaction more attractive. This makes this set of Hamiltonians impractical to extrapolate from at intermediate temperatures as the population of excited states then gets suppressed. The finite χ Hamiltonians affect H_G is such a way as to compensate for this increase in pairing strength. (These Hamiltonians also make the quadrupole-quadrupole interaction, that acts in the particle-hole channel, weaker. This is evident from the dependence of the quadrupole moments on g.)

Double beta decay calculations will be presented for both $\chi = \infty$ and finite χ.

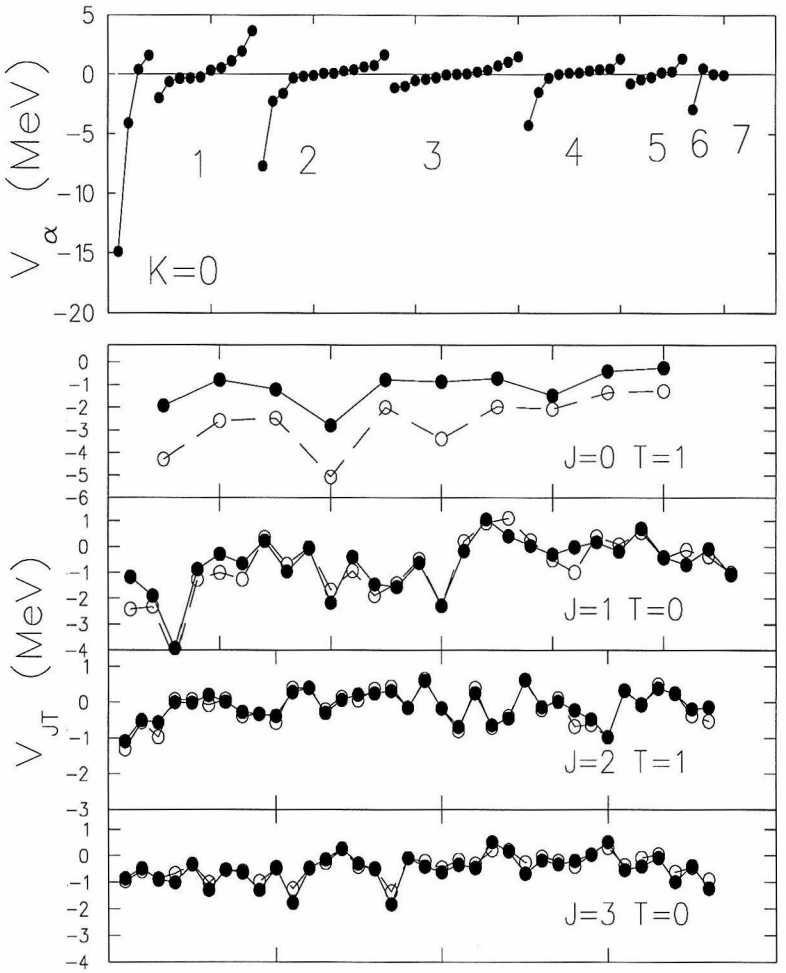

Figure 3.1: Decomposition of the KB3 interaction into good and bad parts. Upper: The V_α. Lower panels: The decomposition in the particle-particle scheme for some representative channels; solid circles are the physical interaction and the open circles are the good pieces. The x-axes number the matrix elements.

3.2 Dynamical correlations and SMMC

In addition to static observables, one can extract strength functions for one-body operators using the SMMC. We calculate the imaginary time response function, $R(\tau)$ ($\tau = n\Delta\beta$ with integer $n \leq N_t$), for an operator $\hat{\mathcal{A}}$ as

$$R(\tau) \equiv \langle \hat{\mathcal{A}}^\dagger(\tau)\hat{\mathcal{A}}(0)\rangle = \frac{\mathrm{Tr}[e^{-(\beta-\tau)\hat{H}}\hat{\mathcal{A}}^\dagger e^{-\tau\hat{H}}\hat{\mathcal{A}}]}{\mathrm{Tr}[e^{-\beta\hat{H}}]} \tag{3.25}$$

$R(\tau)$ is related to the strength function by a Laplace Transform,

$$R(\tau) = \int_{-\infty}^{\infty} S_{\hat{\mathcal{A}}}(E)e^{-\tau E}dE \tag{3.26}$$

where $S_{\hat{\mathcal{A}}}(E) = \sum_{if}\delta(E - E_f + E_i)e^{-\beta E_i}|\langle f|\hat{\mathcal{A}}|i\rangle|^2$ is the strength function for operator $\hat{\mathcal{A}}$ and $|i\rangle$ ($|f\rangle$) are the many-body states of the initial (final) nucleus with energy E_i (E_f).

Using a spectral expansion of $R(\tau)$ as

$$R(\tau) = \frac{\sum_{if} e^{\beta E_i}e^{-\tau(E_f-E_i)}|\langle f|\hat{\mathcal{A}}|i\rangle|^2}{\sum_i e^{-\beta E_i}} \tag{3.27}$$

one can see that for large $(\beta - \tau)$ and τ, $R(\tau)$, measures only the transition between the ground state and the lowest state the operator connects to and thus, in principle, this transition can be measured.

In describing response functions and the $2\nu\beta\beta$ decay "response" we will employ the continous notation for $\hat{U}$, *i.e.*, writing $\tau' = n'\Delta\beta$ and $n > n'$

$$\hat{U}_\sigma(\tau,\tau') = \hat{U}_n \cdots \hat{U}_{n'}. \tag{3.28}$$

In this notation $\hat{U}_\sigma(\beta, 0) \equiv \hat{U}_\sigma$. Then, defining $\hat{\mathcal{A}}(\tau)$ as

$$\hat{\mathcal{A}}(\tau) \equiv \hat{U}_\sigma(\tau, 0)^{-1} \hat{\mathcal{A}} \hat{U}_\sigma(\tau, 0) \tag{3.29}$$

we arrive at the path integral form for $R(\tau)$,

$$R(\tau) = \frac{\int D[\sigma] W(\sigma) \Phi(\sigma) \langle \hat{\mathcal{A}}^\dagger(\tau) \hat{\mathcal{A}}(0) \rangle_\sigma}{\int D[\sigma] W(\sigma) \Phi(\sigma)}. \tag{3.30}$$

For the simplest case, when $\hat{\mathcal{A}} = \hat{a}_i^\dagger$ or $\hat{\mathcal{A}} = \hat{a}_i$, it can be shown [61] from the equations of motion that

$$\hat{a}_i^\dagger(\tau) = \sum_{ij} [\mathbf{U}_\sigma(\tau, 0)^{-1}]_{ij}^T \hat{a}_j^\dagger \tag{3.31}$$

$$\hat{a}_i(\tau) = \sum_{ij} \mathbf{U}_\sigma(\tau, 0)_{ij} \hat{a}_j \tag{3.32}$$

where $\mathbf{U}_\sigma(\tau, 0)$ is the matrix representation of $\hat{U}_\sigma(\tau, 0)$ in the set of single-particle states.

Thus, creation and annihilation operators (and hence any one-body operator) can be "propagated" back to $\tau = 0$. We then define for any one body operator $\hat{\mathcal{A}} = \sum_{ij} \mathbf{A}_{ij} \hat{a}_i^\dagger \hat{a}_j$ (where $\mathbf{A}_{ij}$ is the single particle matrix elements of $\hat{\mathcal{A}}$), which can be evaluated as

$$\hat{\mathcal{A}}(\tau) = [\mathbf{U}_\sigma(\tau, 0)^{-1} \mathbf{A} \mathbf{U}_\sigma(\tau, 0)]_{ij} \hat{a}_i^\dagger \hat{a}_j. \tag{3.33}$$

$R(\tau)$ can then be calculated using static one and two body densities and propagated single particle matrix elements of $\hat{\mathcal{A}}$.

This implementation requires a loop over all the single particle states for the

four indices in $R(\tau)$ and thus scales as $(N_s)^4$. (The propagation of A_{ij} requires two multiplications and thus scales only as $2N_s^3$). Later, in section 3.3 we will see that our approach to $2\nu\beta\beta$ decay requires similar functions but they will be implemented very differently to speed up the calculation.

We now return to a discussion of maximum entropy used to recover strength functions from $R(\tau)$.

3.2.1 Method of Maximum Entropy

The inverse Laplace transform required to extract the strength functions is an ill-conditioned numerical problem. The kernel (which in this case is $e^{-\tau E}$) acts as a smoothing operator and thus the solution which requires an inversion will be extremely sensitive to small changes, *i.e.*, errors in the input data. In what follows, a procedure based on the idea of Maximum Entropy is used to perform this transformation.

Consider the χ^2-deviation of the data, $r_i \equiv R(\tau = i\Delta\beta)$, with errors, σ_i, from the fit values $F_i\{S\}$ obtained according to Eq. (3.26) as,

$$\chi^2\{S\} = \sum_i \left(\frac{r_i - F_i\{S\}}{\sigma_i}\right)^2 . \tag{3.34}$$

Direct minimization of χ^2 is numerically stable in only the simplest of circumstances such as few-parameter data fitting. Combining χ^2 with some other auxiliary well-conditioned functional, $P\{S\}$ such that $P\{S\}$ has a minimum at the smooth solution, $S(E)$ and penalizes strongly oscillating functions leads to a compromise between fitting the data and the expected smoothness of the inverse.

Thus one minimizes the joint functional

$$\frac{1}{2}\chi^2\{S\} + P\{S\} \ . \tag{3.35}$$

The functional, $P\{S\}$ is chosen as the entropy from information theory as,

$$P\{S\} = \alpha \int dE \left[m(E) - S(E) + S(E) \ln\left(\frac{S(E)}{m(E)}\right)\right] \ , \tag{3.36}$$

where $m(E)$ is the default model and α is an adjustable parameter which specifies one's *a priori* knowledge of the function to be recovered. We choose a Gaussian for $m(E)$ with the centroid appropriately chosen (see section 4.1) and an arbitrary width of 2 MeV. The parameter α is chosen from some known sum-rule, in this case α is given in terms of the total strength, $\alpha = [\int dE m(E)]^{-1}$.

In order to minimize the functional (Eq. (3.35)) we employ the technique of Ref. [62], which involves an iterative sequence of linear programming problems. To do this we first expand Eq. (3.36) to second order in $S(E)$ about some positive function $f(E)$, to obtain

$$P\{f \mid S\} = \alpha \int dE \left\{ \left(m - \frac{f}{2}\right) + \left[\ln\left(\frac{f}{m}\right) - 1\right] S + \frac{S^2}{2f} \right\} \ . \tag{3.37}$$

If the true minimum $S(E)$ of the non-quadratic functional in Eq. (3.36) is taken as a point of expansion $f(E)$ in (Eq. (3.37)), then it also gives the minimum of the corresponding quadratic functional

$$S(E) = \min_a \left[\frac{1}{2}\chi^2\{a\} + P\{S \mid a\}\right] \ . \tag{3.38}$$

Since we require to extract a positive strength function, we iterate keeping the

result of the previous iteration partially as,

$$S^{(n+1)} = \min_{S \geq 0} \left[\frac{1}{2} \chi^2 \{S\} + P\left\{ f^{(n)} \mid S \right\} \right] , \tag{3.39}$$

with

$$f^{(n)}(E) = \xi S^{(n-1)}(E) + (1 - \xi) S^{(n)}(E) , \tag{3.40}$$

and the default model as the starting approximation to S,

$$S^{(0)}(E) = S^{(-1)}(E) \equiv m(E) . \tag{3.41}$$

The rate of convergence and stability are controlled by the mixing parameter ξ where $0 < \xi < 1$; a value of $\xi = 0.3$ is a reasonable choice to guarantee stability. Typically, convergence to the "true" solution is obtained in less than 40 iterations.

Thus, the minimization of a general functional that is intrinsic to a Maximum Entropy approach is reduced to an iteration procedure with each step requiring the minimization of a quadratic functional with linear inequality constraints. This procedure is used to obtain the results presented in section 4.1.

We now turn to the matrix element of $2\nu\beta\beta$ decay which is yet another kind of quantity that can be calculated using the SMMC.

3.3 Two neutrino double beta decay

The SMMC does not explicitly enumerate the various states of the nucleus. Thus, we do not have the transition matrix elements between individual states and the sum in Eq. (2.10) cannot be explicitly evaluated. However, we can get information regarding the excited states through response functions and thus, we will define

similar functions from which to calculate the 2ν matrix element.

To calculate the $2\nu\beta\beta$ matrix element, Eq. (2.10), we consider the function

$$\phi(\tau,\tau') = \frac{\mathrm{Tr}[e^{-(\beta-\tau-\tau')\hat{H}}\hat{\mathbf{G}}^\dagger \cdot \hat{\mathbf{G}}^\dagger e^{-\tau\hat{H}}\hat{\mathbf{G}}e^{-\tau'\hat{H}} \cdot \hat{\mathbf{G}}]}{\mathrm{Tr}[e^{-\beta\hat{H}}]}. \tag{3.42}$$

where $\hat{H}$ is the many-body Hamiltonian and the trace is over all states of the initial nucleus. Note that this function is equivalent to replacing $\hat{\mathbf{G}}$ by $\hat{\mathbf{G}}^\dagger$ and performing the many-body trace over all the states of final nucleus instead of the initial nucleus.

The quantities $(\beta-\tau-\tau')$ and τ play the role of the inverse temperature in the parent and daughter nucleus respectively.

Using the definition of $\hat{\mathbf{G}}(\tau)$ given in Eq. (3.29) one has an expression suitable for Monte Carlo evaluation as,

$$\phi(\tau,\tau') = \frac{\int D[\sigma]W(\sigma)\Phi(\sigma)\langle\hat{\mathbf{G}}^\dagger(\tau+\tau')\hat{\mathbf{G}}^\dagger(\tau+\tau')\hat{\mathbf{G}}(\tau)\mathbf{G}\hat{(\mathbf{0})}\rangle_\sigma}{\int D[\sigma]W(\sigma)\Phi(\sigma)}. \tag{3.43}$$

We will return to the details of how ϕ is implemented in the next section where we will discuss the computational aspects of such a calculation.

To see how one can obtain $M^{2\nu}$ from ϕ consider a spectral expansion of ϕ. One has,

$$\phi(\tau,\tau') = \frac{\sum_{if} e^{-(\beta-\tau-\tau')E_i}\langle i|\hat{\mathbf{G}}^\dagger \cdot \hat{\mathbf{G}}^\dagger|f\rangle e^{-\tau E_f}\sum_m e^{-\tau' E_m}\langle f|\hat{\mathbf{G}}|m\rangle\langle m|\hat{\mathbf{G}}|i\rangle}{\sum_i e^{-\beta E_i}} \tag{3.44}$$

where $|i\rangle$, $|f\rangle$, and $|m\rangle$ are the many-body states with energies E_i, E_f, and E_m in the initial, final and intermediate nucleus. In the limit of large β, $(\beta-\tau-\tau')$, and τ one cools to the ground state of the initial and final even-even nucleus (which are both 0^+ and thus the GT operator connects only to 1^+ states in the intermediate

nucleus) and thus obtains

$$\phi(\tau,\tau') = e^{(\tau+\tau')E_i^0} e^{-\tau E_f^0} \langle 0_i^+|\hat{\mathbf{G}}^\dagger \cdot \hat{\mathbf{G}}^\dagger|0_f^+\rangle \sum_m e^{-\tau' E_m} \langle 0_f^+|\hat{\mathbf{G}}|1_m^+\rangle \cdot \langle 1_m^+|\hat{\mathbf{G}}|0_i^+\rangle \quad (3.45)$$

where E_i^0 and E_f^0 are the energies of the ground states of the initial and final nucleus respectively. In these limits, we note that $\phi(\tau,\tau'=0)$ approaches $e^{-\tau Q}|M_c|^2$, where $Q = E_i^0 - E_f^0$ (also called T_0 in chapter 2) is the energy release, so that a calculation of $\phi(\tau,0)$ leads directly to the closure matrix element. If we then define

$$\begin{aligned} \eta(T,\tau) &\equiv \int_0^T d\tau' \phi(\tau,\tau') e^{-\tau' Q/2} \qquad (3.46) \\ &= e^{-\tau Q} M_c^* \sum_m \frac{\langle 0_f^+|\hat{\mathbf{G}}|1_m^+\rangle \cdot \langle 1_m^+|\hat{\mathbf{G}}|0_i^+\rangle}{E_m - (E_i^0 + E_f^0)/2} \times [1 - e^{-T(E_m - (E_i^0+E_f^0)/2)}] \end{aligned}$$

and

$$M^{2\nu}(T,\tau) \equiv \frac{\eta(T,\tau) M_c}{\phi(\tau,0)}, \qquad (3.47)$$

it is easy to see that in the limit of large τ, $(\beta - \tau - \tau')$, and T, $M^{2\nu}(T,\tau)$ becomes independent of these parameters and is equal to the matrix element in Eq. (2.10).

A brief discussion about the choice of parameters β, τ, and τ' is in order here. To make this choice, we note that one can obtain a rough estimate of the excitation energy corresponding to a temperature $T = \beta^{-1}$ MeV (not to be confused with the parameter T in Eq. 3.47) from fermi-gas level densities [63]. (This, of course, is not appropriate for the low-energy spectra due to the neglect of correlation effects associated with collective modes of excitation. However, it is adequate for a rough estimate.) This energy, E, scales roughly as $E \sim aT^2$ (where a, the level density parameter is $a \sim A/8$ empirically). Thus, for $A = 50$, $E \sim 6T^2$.

For the pf-shell even-even nuclei, using the experimental spectrum as a guide (we assume that our calculation faithfully reproduces the experimental levels!) the first excited state is at least 1 MeV above the ground state and $\beta = 2$ MeV^{-1} has been shown to be sufficient to obtain ground state properties [28]. One can in addition, use expectation value of quantities like the angular momentum, J^2, as an indicator of the admixture of excited states in the calculation.

The parameter τ is an inverse temperature in the final nucleus which is also even-even. However, τ need not be as large as β because the $\hat{\mathbf{G}} \cdot \hat{\mathbf{G}}$ operator is a scalar operator and thus connects the 0^+ states in the initial nucleus to only 0^+ states in the final nucleus. The first excited 0^+ state in even-even nuclei is typically at higher energies than the first excited state and so a higher temperature, *i.e.*, $\tau < \beta$ is sufficent to cool to the ground state. Again, for the same reason $(\beta - \tau)$ (in the initial nucleus) need not be as large as β.

The parameter τ' tracks the energies of the 1^+ states in the intermediate nucleus. Thus, the function ϕ needs to be calculated for several values of τ' till the integral, η, converges.

We use SMMC methods to calculate $\phi(\tau, \tau')$, and hence $M^{2\nu}$ and these details are discussed in the next section.

3.3.1 Computational considerations

The $2\nu\beta\beta$ "response function", $\phi(\tau, \tau')$, can, in principle, be calculated using the same methods as the ordinary response function, $R(\tau)$. However, the SMMC approach to $\beta\beta$ decay requires a four-body operator. Hence, the loop over single-particle states scales as $(N_s)^8$ making even a pf-shell calculation unfeasible. Instead, we implement $\phi(\tau, \tau')$ exploiting symmetries in the operator in the following

way.

We write $\hat{\mathbf{G}}$ as $\hat{\mathbf{G}} = \sum_{ij} \boldsymbol{\sigma}_{ij} \pi_i^\dagger \nu_j$ (i and j are indices running over N_s single particle states and π ν stand for proton and neutron respectively) and note that we need to evaluate the operator in the expectation value in the integrand in Eq. (3.43).

To demonstrate the symmetries in this operator consider the static operator corresponding to $\phi(0,0)$.

$$\hat{\mathbf{G}}^\dagger \cdot \hat{\mathbf{G}}^\dagger \hat{\mathbf{G}} \cdot \hat{\mathbf{G}} = \sum_{ijklabcd} (\boldsymbol{\sigma}_{ij} \cdot \boldsymbol{\sigma}_{kl})(\boldsymbol{\sigma}_{ab} \cdot \boldsymbol{\sigma}_{cd}) \nu_i^\dagger \pi_j \nu_k^\dagger \pi_l \pi_a^\dagger \nu_b \pi_c^\dagger \nu_d. \tag{3.48}$$

This operator is antisymmetric in the single-particle indices (i and k), (j and l), (a and c), and (b and d). Thus, we can restrict the sum to only terms that contribute once. In addition, we loop only over the non-zero $C_{ijkl} \equiv \boldsymbol{\sigma}_{ij} \cdot \boldsymbol{\sigma}_{kl}$. This reduces the size of the loop by orders of magnitude ($\sim 10^5$ in the pf-shell).

Since the $\mathbf{U}$ matrices mix all the single-particle states, this implementation precludes using the scheme used in the "propagation" of the single-particle matrix elements for the response functions. Instead, we propagate the one and two-body densities. We do not give detailed formulae here as this propagation simply involves multplying the γ matrices in Eq. (3.23) by the corresponding $\mathbf{U}$ matrices and then calculating the densities through Eq. (3.20) and Eq. (3.21) for each set of τ and τ'.

Even though a significant fraction of the computational effort in the SMMC goes into calculating the two-body densities ($\sim$ 15%), this scheme for $\phi(\tau, \tau')$ results in a considerable speed-up of the calculation as the innermost loop over single-particle states is now significantly smaller and can be vectorized. Approximately, 80% of the computational effort is spent in the evaluation of $\phi(\tau, \tau')$ in

the pf-shell for one value of τ and ten values of τ'.

Chapter 4 Results and Discussion

In this chapter, we first demonstrate the maximum entropy method for obtaining strength functions (see section 3.2) for various nuclei [64] in the pf-shell including (p,n) for ^{48}Ca and (n,p) for ^{48}Ti, the cases relevant for $\beta\beta$ decay of ^{48}Ca. We also briefly talk about an ongoing project to calculate electron capture rates at relevant temperature of a supernova core. We then demonstrate our method for obtaining the 2ν matrix element [65] for the decay of ^{48}Ca and validate it against direct diagonalization using a code based on the Lanczos method. We then discuss this result in the light of the experimental half life using direct-diagonalization [66]. We also discuss the issue of the contributions to the 2ν matrix element from the various 1^+ states in the intermediate nucleus. and then apply the SMMC method to the decay of ^{76}Ge.

4.1 GT strength functions for pf-shell nuclei

4.1.1 GT strength distributions and 2ν decay of ^{48}Ca

The matrix element, $M^{2\nu}$ is equivalent to a full description of the strength functions of the β^- decay of the initial and β^+ decay of the final nucleus. Thus, any reliable calculation of $M^{2\nu}$ must be able to describe the relevant strength functions appropriately.

In the lower leftmost panel of Fig. (4.1), we show the β^+ response function, $R(\tau)$, for ^{48}Ti. From Eq. (3.27), one can see that $d\ln[R(\tau)]/d\tau|_{\tau=0}$ gives the cen-

troid of the distribution in the parent nucleus and thus we choose a Gaussian with a peak at this energy and with an arbitrary width of 2 MeV for the default model in the Maximum Entropy extraction of the strength function in the daughter, ^{48}Sc (shown in the middle lower panel). Also shown in the same panel is the direct-diagonalization result. The SMMC can recover only gross features of this distribution however, the SMMC $B(GT_+) = 1.13 \pm 0.18$ [28] compares very well with the direct-diagonalization value of 1.26. Since $R(\tau)$ is calculated at discrete values of imaginary time and in principle upto an imaginary time β, the smallest energy that can be resolved in $S(E)$ is of order $1/\beta$ and the largest is the inverse of the discretization size, $1/\Delta\beta$. From the lower rightmost panel, where the cumulative strength versus energy in the daughter is shown, one can see that the SMMC recovers the centroid and the width of the distribution very well.

A brief note about the statistical and the possible physical sources of error is in order here. Since our method provides a most probable extraction of the strength function, these functions do not have error bars associated with them. However, using the SMMC error bars for $R(\tau)$, one can estimate the error in the position of the centroid to be about 1.0 MeV.

The response functions are measured in the parent nucleus and to obtain the energy in the daughter we use the experimental mass excesses and a parametrization of the Coulomb energy as defined in [67]. This parametrization is used to enable comparisons with direct-diagonalization calculations already in the literature [67] and provides an overall good description of the masses of several nuclei in this region. A different phenemenological parametrization, for instance, $E_c = \frac{0.717Z^2}{A^{1/3}}(1 - \frac{1.69}{A^{2/3}})$, (as in Ref. [68]) could yield an energy different by as much as 1.5 MeV. Thus, in comparison with experiments we use the parametrization that yields a consistently good description of the masses of nuclei in this

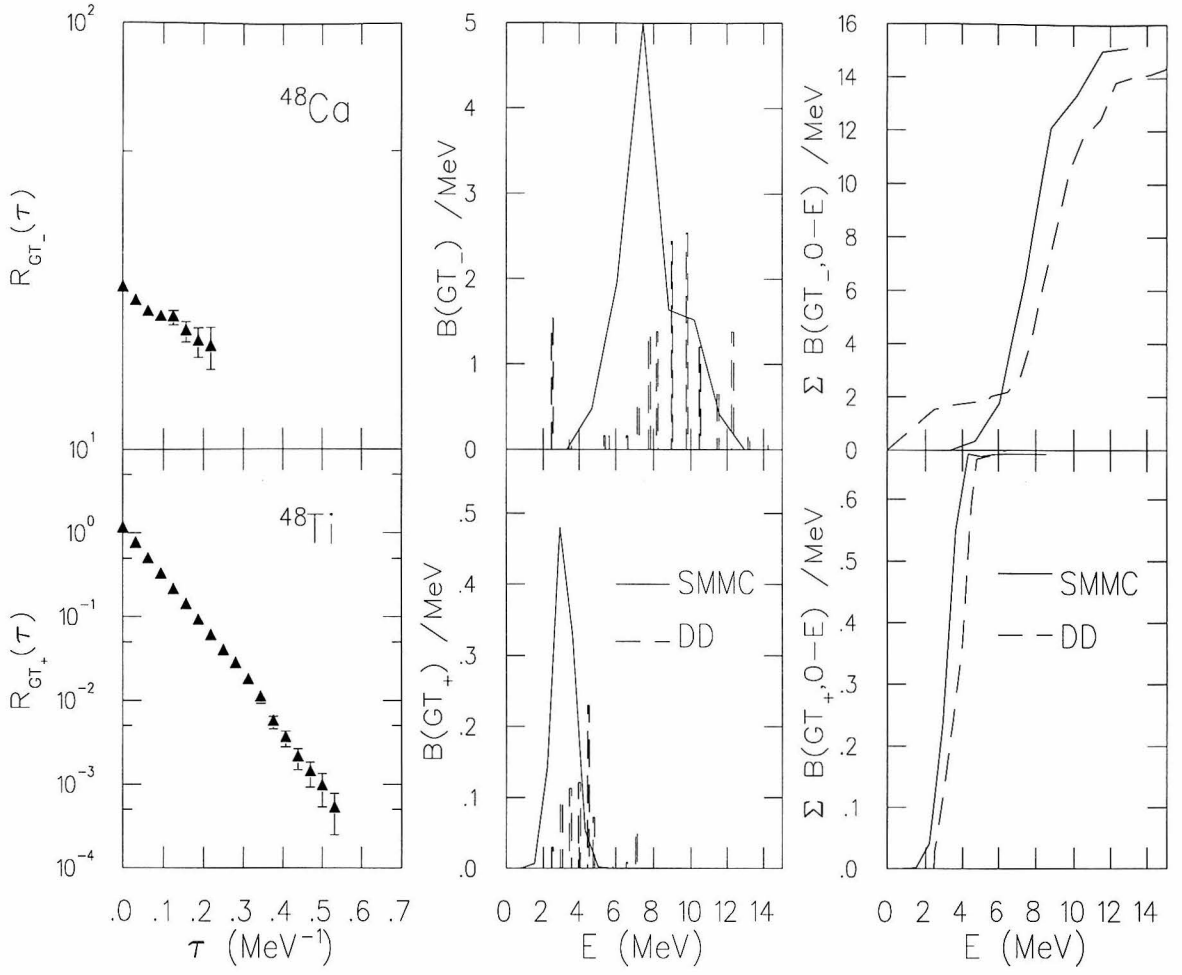

Figure 4.1: Maximum entropy extractions of the GT strength function. Shown in the leftmost panel are the GT response functions versus imaginary time, τ, calculated with the SMMC. The middle panel shows the comparison of the GT strength function in the (p,n) direction for ^{48}Ca and the (n,p) direction for ^{48}Ti in the respective daughters with direct-diagonalization results obtained from Ref. [34]. The rightmost panels show the cumulative strengths for the strength functions also against direct-diagonalization.

region [67].

The upper panels show the same quantities for the β^- decay of ^{48}Ca to ^{48}Sc. In this case, only τ values of upto 0.25 MeV^{-1} are used to obtain the strength function as the GT response is swamped with noise for larger τ values, evident from the SMMC errors. Since, the large τ values dominantly contain information regarding the low-lying states as explained in section 3.2, we see in the comparison against direct-diagonalization that we are unable to recover the low-lying peak at 2.52 MeV. However, a comparison of the cumulative strengths versus energy in the daughter reveals that apart from an overall shift of $\simeq$ 1.5 MeV the SMMC recovers the direct-diagonalization results.

Note that the β^+ of ^{48}Ti and β^- of ^{48}Ca distribute their strengths around significantly different energies, as mentioned earlier. This small overlap is empirically consistent with the small value of the 2ν matrix element.

In Fig. (4.2), we compare the strength distribution of β^+ of ^{48}Ti with the experimental distribution obtained visually from Ref. [69]. The SMMC $B(GT_+)$ (area under the curve) is renormalized by $1/(1.26)^2$ and the SMMC distribution from Fig. (4.1) is smeared out by associating the individual energies in Fig. (4.1) with Gaussians of width of 1.77 MeV normalized to the strength at the energy to accomodate the experimental resolution of 1 MeV. We see from a comparison of the SMMC result with experiment that there is considerable high energy strength in the experiment that is missing in the calculation. Experimental distributions typically include a cut-off at about 8 MeV to eliminate dubious strength due to backgrounds; a procedure apparently not followed in this case. If Gamow-Teller, this high-lying strength points to the insufficiency of the model space in the calculation. The obvious extension of this calculation involves one with the sd and pf model space. Such multi-shell calculations that may resolve this issue are

computationally feasible within the SMMC. The pf-shell result from the SMMC for the $B(GT_+)$ of 1.13 ± 0.18 is to be compared with the experimental strength of 1.31 ± 0.2 (up to 15 MeV).

The SMMC result for the centroid and width of the distribution of β^- strengths of ^{48}Ca compares well with the experimental distribution [70]. The $B(GT_-)$ for ^{48}Ca from the SMMC is trivially 24 from the model-independent GT sum rule. However, since the absolute heights of the peaks in the experimental distribution are not known, we cannot perform a detailed comparison with the SMMC result.

4.1.2 GT strength distributions and supernovae studies

Gamow-Teller strengths play an important role in determining the size of presupernova core at collapse. After silicon burning, pf-shell nuclei become abundant in the core of a star. Because of the high density of this core ($> 10^7 \mathrm{gm/cm}^3$) electrons become highly degenerate and the large Fermi energy of these electrons enables them to excite GT strength in these nuclei. As recognized by Bethe *et al.* [71] electron capture rates on these nuclei can be dramatically enhanced thus affecting the temporal evolution of Y_e (the charge to mass ratio of the star) which in turn determines the mass of the core at collapse. In addition, neutrinos that are products of such reactions can transport energy out of the core and thus affect its final collapse.

Shown in Fig. (4.3) are the β^+ strength functions against experiment for the nuclei - ^{60}Ni, ^{58}Ni, ^{56}Fe, and ^{54}Fe [72, 73]. The SMMC distributions are smeared out as for ^{48}Ti (described in the previous subsection). The SMMC recovers the peak and the width of these distributions well.

Also, Fig. (4.4) shows the β^- GT strength distribution against experiment ob-

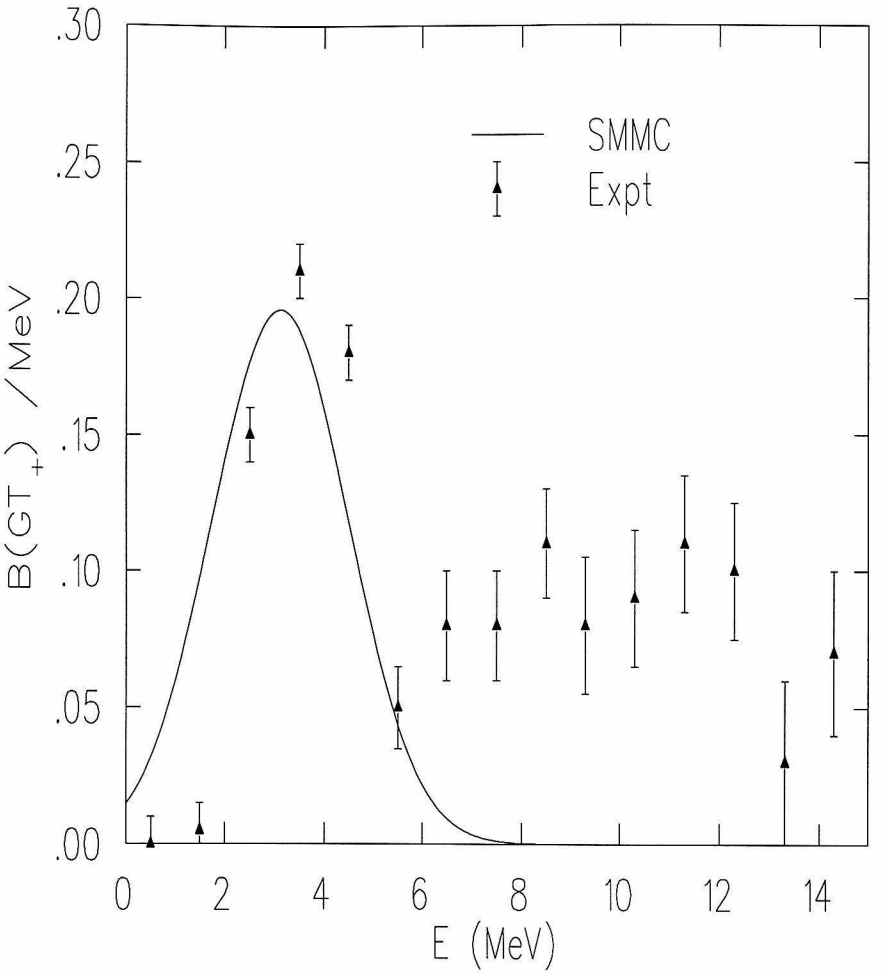

Figure 4.2: Comparison of the SMMC strength function with experiment for ^{48}Ti in the (n,p) direction [69]. Note that there is considerable high-energy strength missing in the calculation.

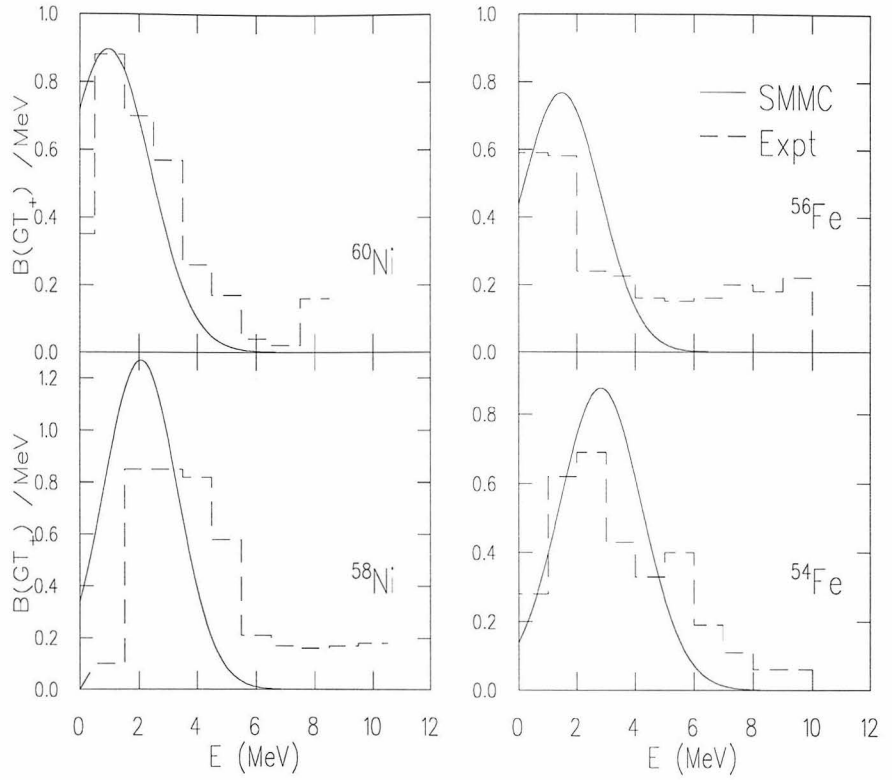

Figure 4.3: Comparison of the SMMC β^+ strength function with experiment for ^{60}Ni, ^{58}Ni, ^{56}Fe, and ^{54}Fe. Note that these strengths are distributed over many states.

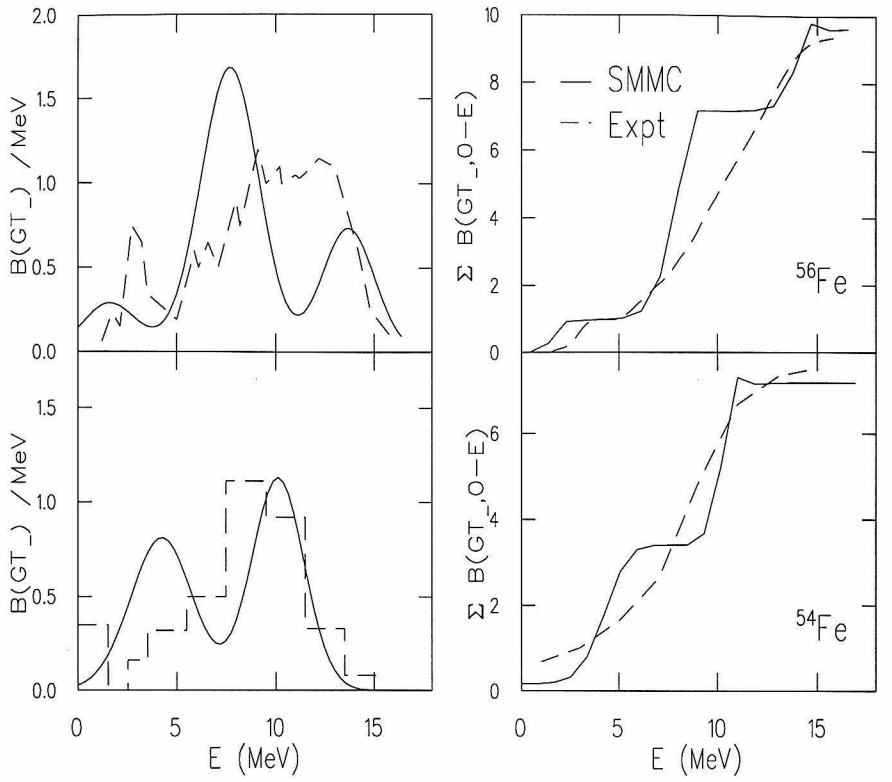

Figure 4.4: Left panels: Comparison of the β^- SMMC strength function with experiment for ^{56}Fe and ^{54}Fe. Right panels: Cumulative strengths for the corresponding nuclei.

tained in (p, n) reactions for ^{56}Fe and ^{54}Fe [74, 75] (left panels) and the cumulative strengths (right panels).

Inputs to supernovae codes are based on the first estimates of the GT strength by Fuller, Fowler, and Newman (FFN) (see for instance, Ref. [76]) who used the independent particle model to estimate the total strength and placed all of it in one state. Fig. (4.3) shows that this strength is highly fragmented and phase space considerations make the electron capture rates extremely sensitive to the GT strength distribution. Thus, a reliable calculation of these rates is imperative to remove uncertainties related to presupernova evolution.

SMMC response functions are being used to obtain GT strength distributions for about thirty of the important nuclei relevant to this problem. Not only can these quantities be obtained for realistic model spaces and interactions but can also be calculated for finite core temperatures ($T \sim 0.7$ MeV).

In the following paragraph, the temperature evolution of the GT strength function is discussed briefly. Shown in the lower panel of Fig. (4.5) is a representative temperature dependence in the parent (for the case of ^{60}Ni). As temperature increases, the peak of the distribution shifts to lower energies and the distribution broadens developing pronounced strengths at lower energies. This is most likely due to back transitions from excited states; a feature any reliable finite temperature calculation must have. At zero temperatures only the ground state is populated and the only transitions possible are from the 0^+ ground state (for even-even nuclei) to excited 1^+ states. At finite temperatures, the excited states are also populated and thus transitions from these states to the less excited states occur. These latter transitions have a very different τ dependence in the response function (a rising exponential instead of a falling one; see Eq. (3.27)) and a bump at lower energies in the corresponding strength functions (Fig. (4.5)).

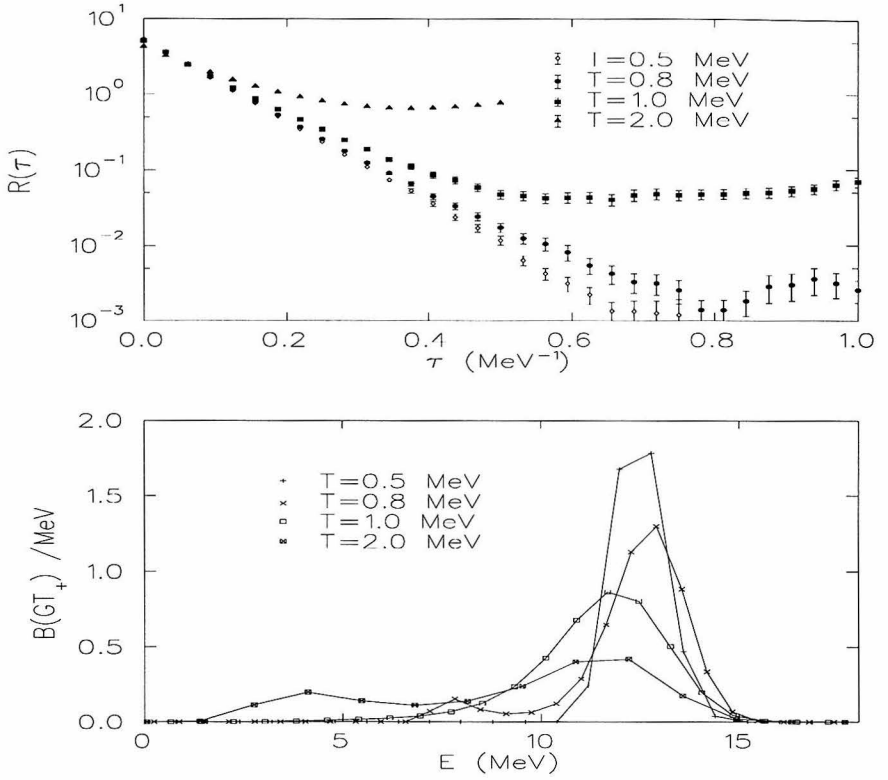

Figure 4.5: Upper: GT response function for ^{60}Ni for various temperatures. Lower: The corresponding strength functions.

Since such calculations are still ongoing, we do not discuss them any further and instead turn to a discussion of the results for $2\nu\beta\beta$ decays.

4.2 Case of ^{48}Ca

^{48}Ca is the lightest of all $\beta\beta$ candidates known. This decay has an extremely favourable energy release of $T_0 = 4.29$ MeV. However, the matrix elements governing this transition are unusually weak and with a natural abundance of only 0.19% ^{48}Ca is a less suitable testing ground for studying $\beta\beta$ decay than its energy release might suggest. We use this case to test the SMMC approach, since this decay can be treated realistically through direct-diagonalization methods, *i.e.*, one can solve the problem of eight nucleons in the pf-shell without truncation using these methods [67].

To validate our method, we calculate the matrix elements for ^{48}Ca in the complete pf-shell with the KB3 interaction [67] for six equally spaced g values between -1.0 and 0.0 using $\chi = 4$ and extrapolate to the physical result at $g = 1$. Each calculation involves 2500-3500 Monte Carlo samples and is performed at $\beta = 2$ MeV^{-1} with $N_t = 48$. The direct diagonalization calculations for ^{48}Ca with which we compare our results are performed using an implementation of the Lanczos algorithm [77]. We calculate both the closure and exact matrix elements for the same Hamiltonians, $H(g, \chi)$, as used in the SMMC.

4.2.1 SMMC and 2ν closure matrix element

We calculate the closure matrix element from the function $\phi(\tau, 0)$ (as in Eq. (3.45)) and find the slope of $\ln[\phi(\tau, 0)]$ to be in agreement with that expected from the difference of the energies for ^{48}Ti and ^{48}Ca, Q, (Table 4.1) and extract $|M_c|$ from

Table 4.1: Comparison of SMMC and direct diagonalization values of the difference in energies for the initial and final nucleus for the various g values (all energies in MeV).

g	Q_{DD}	Q_{SMMC}
0.0	13.35	12.87 ± 0.19
-0.2	12.5	11.88 ± 0.24
-0.4	11.64	11.07 ± 0.29
-0.6	10.82	9.85 ± 0.25
-0.8	10.01	9.21 ± 0.29
-1.0	9.48	8.81 ± 0.28

the intercept.

The SMMC closure matrix elements for $g \leq 0$ are in very good agreement with the direct diagonalization results (Fig. (4.6)) indicating that our temperatures are sufficiently low to calculate correctly the closure matrix element from the ground state of ^{48}Ca to ^{48}Ti. However, the direct diagonalization calculations show a small curvature near $g = 1.0$ that the extrapolation cannot reproduce. Our linear extrapolation of the closure matrix element, which takes place over almost a factor of 20, therefore underestimates the physical ($g = 1.0$) calculation. We obtain -0.21 ± 0.29 for the closure matrix element to be compared with the direct diagonalization result of 0.29. As the natural scale for M_c is given by the sum rule (see 2.2) as ≈ 21, we may conclude that the SMMC successfully reproduces the shell model suppression of a factor of 70.

4.2.2 SMMC and 2ν exact matrix element

The calculation of the function $\phi(\tau, \tau')$ is performed for $\tau = 0.5$ MeV^{-1} and for thirteen τ' values spaced equally between 0.0 and 0.5 MeV^{-1}. This combination

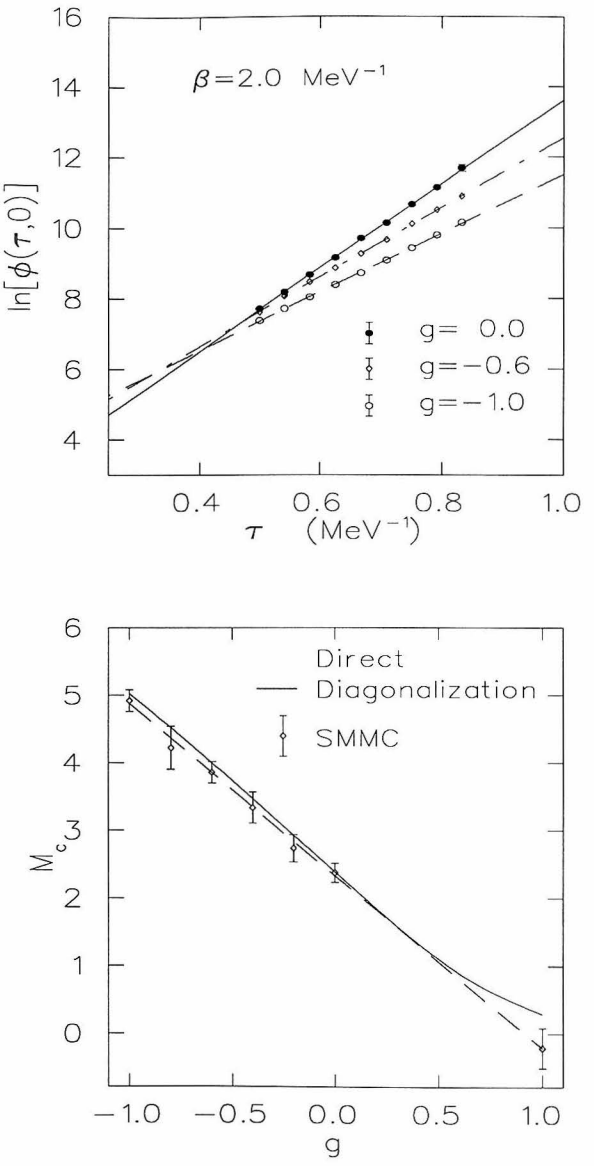

Figure 4.6: Upper: $\ln[\phi(\tau,0)]$ for ^{48}Ca calculated at $\beta = 2.0$ MeV^{-1} with $N_t = 48$. The lines are best fits. Lower: SMMC and direct diagonalization closure matrix elements for ^{48}Ca. The SMMC points are linearly extrapolated to $g = 1.0$.

of parameters has been checked to give converged results for the matrix element. Then, using the known values of Q (from the slope of $\phi(\tau, 0)$, shown in Table 4.1) we obtain the quantity $e^{-\tau' Q/2}\phi(\tau, \tau')$ which is the integrand in Eq (3.46) (shown for some representative values of g in Fig. (4.7)). This function becomes increasingly noisy for larger values of τ' and this numerical noise forces a cut-off in the calculation for η at a value of $\tau' \sim 0.5$ MeV^{-1}. We calculate $\eta(T, \tau)$ for thirteen values of $T \leq 0.5$ MeV^{-1}; the upper limit of T is sufficiently large for the integral in Eq. (3.46) to converge.

To determine the asymptotic ($T \to \infty$) value of $M^{2\nu}(\tau, T)$ (as in Eq. (3.47)) we note that the true functional form of this quantity (from Eq. (3.46)) in T is a linear combination of exponentials with coefficients as the $2\nu\beta\beta$ amplitudes to the mth 1^+ state in the intermediate nucleus as

$$M_m^{2\nu} = m_m^{2\nu}/(E_m - (E_i^0 + E_f^0)/2) \tag{4.1}$$

where $m_m^{2\nu}$ has been defined in Eq. 2.7 and the corresponding energy denominators in the exponent. Since this fit will then involve more parameters than the number of data points due to the low values of τ where exponentials corresponding to all the energy denominators will contribute we use the following procedure to determine the asymptotic value of $M^{2\nu}(\tau, T)$. We construct an ensemble of Gaussian-distributed $\phi(\tau, \tau')$ with mean and standard deviations as calculated in SMMC. Each $M^{2\nu}(\tau, T)$ (with the error as a small random noise) is then fit to the form $a - be^{-cT}$ between $T = 0.17$ MeV^{-1} and $T = 0.5$ MeV^{-1}, and the average and standard deviation of a gives the required matrix element and its error (shown at large T in the upper panel of Fig. (4.8) for some representative values of g). Since there are a large number of such fits we do not show them. Instead, the lines in

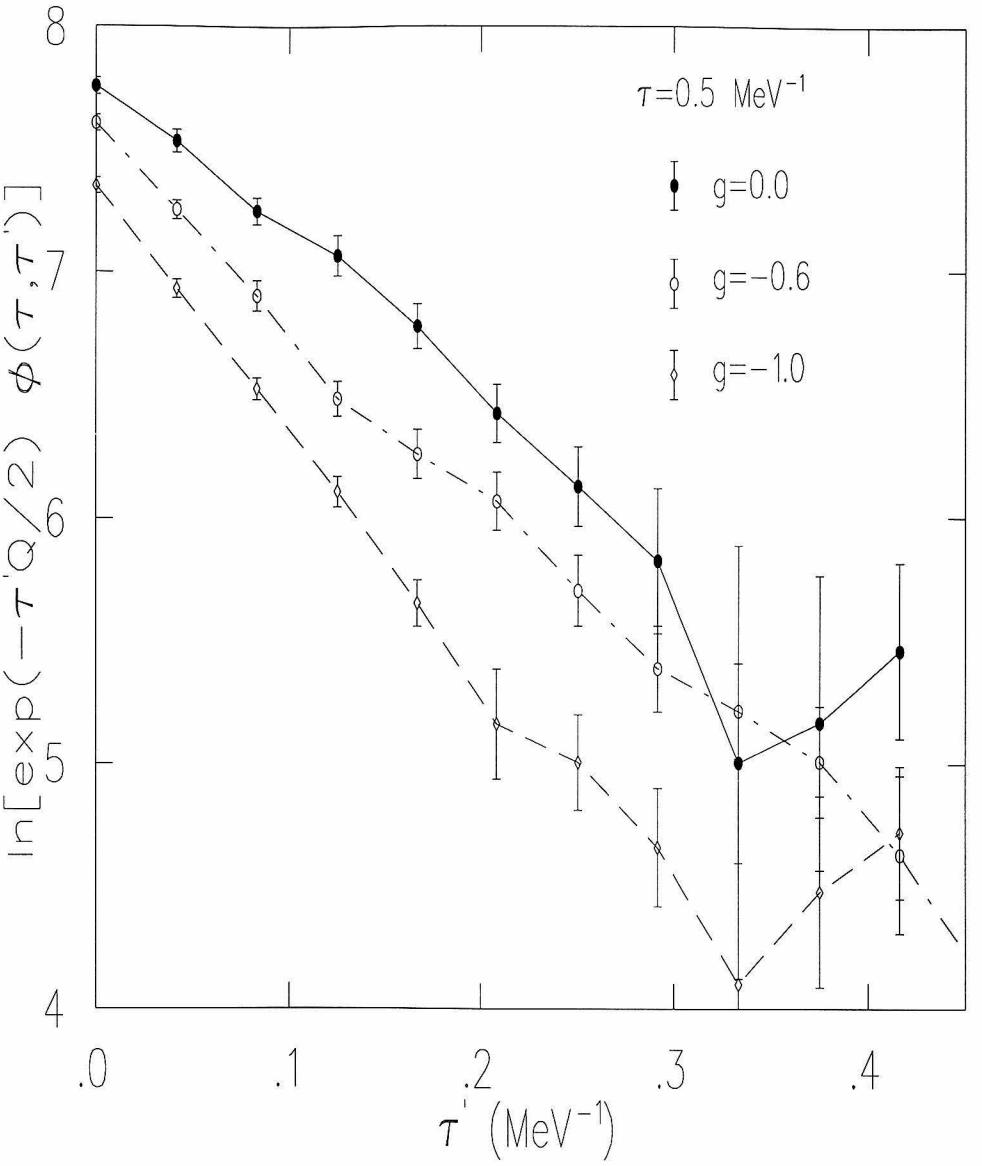

Figure 4.7: Shown in the figure is the natural log of the integrand of Eq. (3.46), $\ln[e^{-\tau' Q/2}\phi(\tau,\tau')]$ for some representative values of g for the case of ^{48}Ca.

Fig. (4.8) are drawn to guide the eye. This functional form provided a very good fit for $M^{2\nu}(\tau, T)$ with χ^2/dof between 0.3 and 1.1 for all the fits.

In calculating $M^{2\nu}$ the standard practice is to shift the lowest 1^+ state [34] to the experimental value. From direct-diagonalization, we know that for the KB3 interaction in this model space, this shift is only 0.1 MeV and amounts to a negligible change in the final numbers. Note that while an overall shift in the energy denominators is possible within the SMMC approach we do not employ it as this quantity is not known for the general g - dependent case.

Being long range the Coulomb interaction can be reasonably well approximated in nuclei by an overall shift to the shell model energies. This provides another source of the shift in the energy denominators is due to the different Coulomb interaction in the three nuclei. This shift is Z independent and scales essentially as $A^{-1/3}$ and is also of the same size for the ^{48}Ca triad (using the parametrization described in section 4.1), but in the opposite direction, thus causing a negligible change in the matrix element. For heavier nuclei this shift is only smaller because of the $A^{-1/3}$ dependence and so we ignore it altogether.

In Fig. (4.8), we show the good agreement between the SMMC matrix elements and direct diagonalization for $g \leq 0$. The systematic underestimation of $M^{2\nu}$ with decreasing g is most likely due to a large value of the discretization parameter, $\Delta\beta$, used in calculating the many-body propagator. The $\beta\beta$ calculations are performed for the smallest value of $\Delta\beta$ ($\Delta\beta = 1/24$) that permits a noise-free evaluation of $\phi(\tau, \tau')$; a value larger than the usual value of $\Delta\beta = 1/36$ [51].

Even though the value of $\chi = 4.0$ was chosen to make the linear extrapolation as smooth as possible, the direct diagonalization results still have a small curvature. For the exact 2ν matrix element we obtain an extrapolated value of 0.15 ± 0.07 MeV^{-1} whereas the calculation of Caurier *et al.* [34] (including the er-

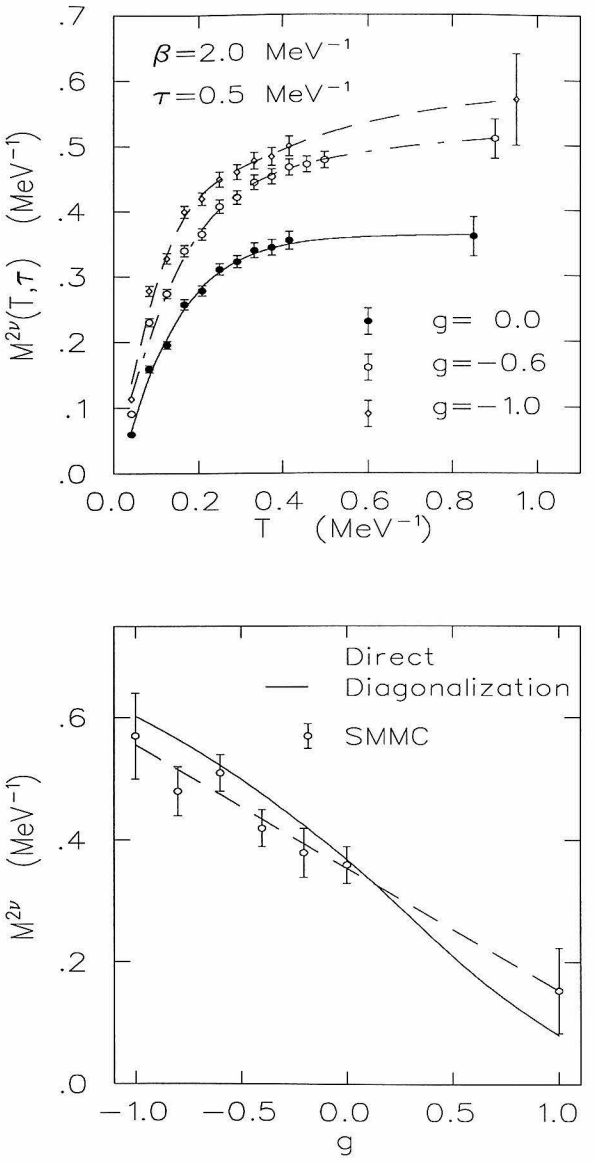

Figure 4.8: Upper: $M^{2\nu}(T,\tau)$ for ^{48}Ca calculated at $\beta = 2.0\ \mathrm{MeV}^{-1}$ with $N_t = 48$. The points at large T show the asymptotic value ($T \to \infty$) of the matrix elements obtained as described in the text; lines are drawn to guide the eye. Lower: SMMC exact matrix elements and the direct diagonalization results for ^{48}Ca. The SMMC matrix elements are linearly extrapolated to $g = 1.0$.

ratum in [67]) gives 0.08 MeV^{-1}. There is thus agreement within the uncertainty.

4.2.3 2ν decay of ^{48}Ca and experiment

Till recently, only a lower limit of the half-life for the 2ν decay was known, $T_{1/2} \geq 3.6 \times 10^{19}$ years [78]. Most calculations give half-lives barely compatible with that restriction. For example, the full pf-shell calculations of Ogawa and Horie [79] predict $T_{1/2} = 3.3 \times 10^{19}$ years (when modified for the in-medium quenching of the Gamow-Teller strength and using the same phase space factor as in [34] for consistency), while Caurier, Poves and Zuker [34] calculate $T_{1/2} = 3.7 \times 10^{19}$ yr (including the erratum in [67]). Similarly, Zhao, Brown and Richter [80] who used a slightly truncated shell model space (allowing utmost 4 nucleons lifted from the $f_{7/2}$ sub-shell in ^{48}Ca and ^{48}Ti, and utmost 5 in ^{48}Sc), obtain $T_{1/2} = 1.9 \times 10^{19}$ yr, in conflict with the experimental limit. (We repeated the calculation without truncation and found that the half-life increase to $T_{1/2} = 2.1 \times 10^{19}$ yr.) In each of these calculations slightly different parameters in the nuclear Hamiltonian were used. All of them, however, were tested by comparing the calculated energy levels, and in particular the GT transition probabilities, with the available data for nuclei at or near $A = 48$.

The agreement with the experimental lower limit [78], albeit marginal, was obtained only when the empirical quenching of the GT strength, *i.e.*, the multiplication of all matrix elements of the operator $\sigma\tau_{\pm}$ by an universal quenching factor $1/(1.26)^2$, is used which as we discussed in section 4.1 may not be applicable to 2ν decay.

The nuclear Hamiltonian for the pf-shell is a set of 195 two-body matrix elements and 3 single-particle energies and is not completely determined. The

question that will be answered in this section is how the half-life can be affected by the uncertainties in the Hamiltonian [66]. This section also serves to illustrate the various physics that can affect the nuclear matrix element.

A similar task was undertaken in Ref. [33]. There, the G-matrix based Paris potential is used as a starting point and the 2ν decay rate is calculated in a truncated shell model. By modifying the pairing, quadrupole, or $J^\pi = 1^+$ components of the nucleon residual interaction, the authors manage to suppress the 2ν decay arbitrarily. However, they do not consider any known properties of the initial, intermediate, and final nuclei, and it is not known whether their modified Hamiltonian is in conflict with them or not. In fact, the $M^{2\nu}$ value in Ref. [33] with the unmodified Hamiltonian is very small, corresponding to a lifetime of 6.4×10^{21} yr, which probably indicates that such a Hamiltonian does not describe the spectroscopy of the $A = 48$ system very well.

Among the various pieces of the Hamiltonian, two components are particularly important for 2ν decay. The pairing interaction, governed by the matrix elements in the $J^\pi, T = 0^+, 1$ channel and the proton-neutron $J^\pi, T = 1^+, 0$ interaction. When pairing is weakened, the deformation of the final nucleus ^{48}Ti increases, and the 2ν matrix element decreases. On the other hand, the attractive proton-neutron interaction controls the β^+ strength of the final nucleus. When this interaction becomes stronger, the β^+ strength and the 2ν matrix element are reduced. Guided by this observation, we choose two parameters, λ^{01} and λ^{10} which scale the relevant matrix elements, in our search for acceptable modifications of the shell model Hamiltonian:

$$\langle a, b|V|c, d\rangle_{J,T=0,1} \quad \rightarrow \quad \lambda^{01}\langle a, b|V|c, d\rangle_{J,T=0,1} \tag{4.2}$$

Table 4.2: Comparison of calculated and experimental values of various indicators for the four cases indicated in Fig.(10) (all energies in MeV).

λ^{01}, λ^{10}	2_1^+ energy in ^{48}Ti	4_1^+ energy in ^{48}Ti	1_1^+ energy in ^{48}Sc	energy denominator $E(1_1^+)$ - $1/2(M_i + M_f)$
experiment	0.98	2.30	2.52	4.37
1.0,1.0	1.03	2.31	2.39	4.51
1.0, 1.2	1.10	2.38	2.21	4.31
0.9, 1.1	0.85	2.02	2.28	4.14
0.9, 1.0	0.82	2.00	2.38	4.22
0.9, 0.9	0.79	1.97	2.47	4.28
1.0, 0.8	0.98	2.26	2.54	4.60

$$\langle a, b|V|c, d\rangle_{J,T=1,0} \quad \rightarrow \quad \lambda^{10}\langle a, b|V|c, d\rangle_{J,T=1,0}$$

Thus, the parameters signify how far the modified Hamiltonian is from the nominal one of Ref. [34] ($\lambda^{01} = \lambda^{10} = 1.0$). We perform the full shell model diagonalization for various values of λ^{01} and λ^{10} using an implementation of the Lanczos algorithm [77]. For each set we evaluate the 2ν matrix element as well as several "indicators" of the goodness of the Hamiltonian as described below.

As expected, $M^{2\nu}$ decreases when $\lambda^{01} < 1$ or $\lambda^{10} > 1$. Thus, by finding the smallest acceptable λ^{01} and the largest acceptable λ^{10} (or their combination) we can obtain a lower limit for $M^{2\nu}$ and thus an upper limit for the 2ν half-life.

The results with the nominal Hamiltonian, and several cases of modified Hamiltonian forming the boundary of the acceptable range of our auxiliary parameters are displayed schematically in Fig. (4.9) and the corresponding indicators are shown in Table 4.2. (Only modifications that potentially lower the value of $M^{2\nu}$ are considered.)

The first 2^+ state in ^{48}Ti is an indicator of the competition between pairing

and quadrupole deformation. As pairing is weakened, *i.e.*, as λ^{01} is decreased, the 2^+ excitation energy decreases. At the same time the 4^+ state, our second indicator, is also lowered and the energy spacings become rotation-like. The parameter λ^{01} also affects the energy denominators of $M^{2\nu}$ since the initial and final even-even nuclei are even more affected by pairing that the intermediate odd-odd nucleus. Therefore, we use the value of the smallest energy denominator as another indicator.

On the other hand, the parameter λ^{10} (related to the parameter g_{pp} used in QRPA) affects primarily the β^+ strength and the excitation energy of the 1^+ states in ^{48}Sc. In Fig. (4.9) we also show the closure matrix element, M_c in order to stress that the ratio $M^{2\nu}/M_c$ is far from constant.

Generally, we demand that the largest deviation from experiment of any of our selected indicators is not more than about 300 keV. This choice is based on the finding that the average deviation between experimental and calculated energies for the nominal Hamiltonian is less that 150 keV for low-lying states in the $A = 48$ system. Thus, our criterion represents 2 standard deviations. We do not use the β^+ strength as an indicator because of issues discussed in section 4.1. Intuitively, among the other combinations,the quadrupole force is expected to play an important role. Since, the quadrupole force acts in the particle-hole channel we cannot use the same procedure as before to test this hypothesis. Instead, we proceed as follows: Starting with the classic quadrupole force $-\kappa\ (\mathcal{Q}_p{}^\dagger + \mathcal{Q}_n{}^\dagger)\ (\mathcal{Q}_p + \mathcal{Q}_n)$ [81] we use the known A-dependence of κ and choose $\kappa = 0.08$ MeV $\cdot$ fm^4, corresponding to approximately a 10% modification of the quadrupole force with the sign chosen such that the attractive force is strengthened. We then use the inverse Pandya transformation and add to the Hamiltonian a set of matrix elements corresponding to this modification.

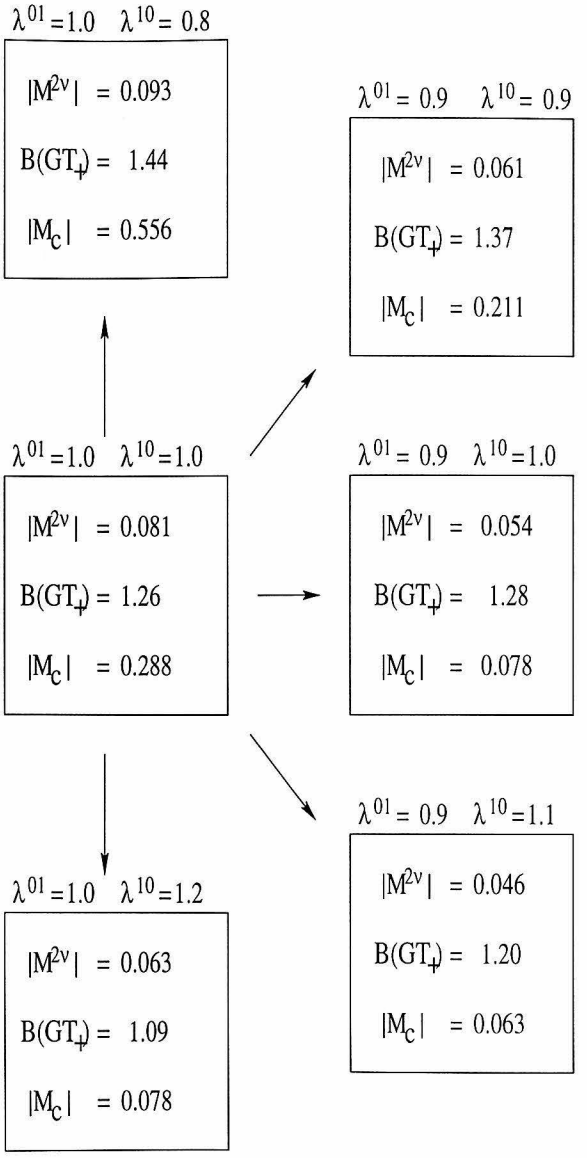

Figure 4.9: Schematic illustration of the six cases considered. In each square we list the most important characteristics, the 2ν matrix element $M^{2\nu}$, (in MeV^{-1}), the total strength $B(GT_+)$, and the closure matrix element M_c. All of them are calculated without the quenching of the $\sigma\tau_\pm$ matrix elements.

Thus, the quadrupole force affects to some degree all the two-body matrix elements. We find that the energy of the 2^+ state is lowered by 0.19 MeV, the 4^+ state is lowered by 0.06 MeV, the 1^+ state is raised by 0.27 MeV, and the first energy denominator is increased by 0.34 MeV with this modificaton. At the same time the β^+ strength is slightly increased to 1.34. As expected, the $M^{2\nu}$ matrix element is decreased to 0.055 MeV^{-1}, and the closure matrix element is decreased to 0.182. Thus, making the quadrupole more attractive is indeed, as far as the 2ν decay is concerned, equivalent to making the pairing weaker. We conclude that the limitations expressed in Fig. (4.9) are rather general.

We checked that inside the area depicted symbolically in Fig. (4.9) the $\beta\beta$ matrix elements are not smaller than at the boundary. Thus, with our (admittedly somewhat subjective) choice of acceptable spectroscopic indicators, we can state that

$$\begin{aligned} M^{2\nu} &\geq \approx 0.05 MeV^{-1} \\ \text{thus}, T_{1/2} &\leq \approx 10^{20} yr \end{aligned} \tag{4.3}$$

where the half-life was obtained with quenched $\sigma\tau_\pm$ matrix elements.

The recent measurement of $T_{1/2}$ of ^{48}Ca due to 2ν decay found a half-life of $T_{1/2} = 5.5^{+3.5}_{-1.5} \times 10^{19}$ yr [13], consistent with this prediction. While, this shows that the shell model can indeed accomodate such lifetimes, it does not resolve the issue of whether the in-medium quenching of g_A is necessary for $\beta\beta$ decay. Stretching the pairing and the $J = 1, T = 0$ components of the interaction maximally, one can avoid the conflict with experiment even without the renomalization of the $\sigma\tau_\pm$ matrix elements.

4.3 $2\nu\beta\beta$ and high-lying GT strength

Another issue in the calculation of $M^{2\nu}$ is the convergence of the sum in excitation energy or in other words, the question of whether there is an energy region in the intermediate nucleus that is responsible for the bulk of the decay.

In Ref. [82] Ericson *et al.*, show that by assuming a random nature of the β^+ and β^- amplitudes, one can conclude that the contribution of the high-lying states to 2ν decay is strongly suppressed and thus this convergence is relatively fast. A similar phenomenon is seen in the decays of ^{100}Mo and ^{128}Te where the intermediate nucleus which happens to be 1^+ carries the bulk of the matrix element. Thus, it is a useful exercise to explore the various contributions to the 2ν strength. To this end, we will use the Lanczos code (also used in section 4.2).

Fig. (4.10) shows the various contributions from the 1^+ states in the intermediate nucleus, $M^{2\nu}_m$ (defined in Eq. (4.1)) to the 2ν matrix element for different values of g. For each g value, only the relative heights and signs from the various 1^+ states matter as the overall phase of the $\beta\beta$ amplitude is arbitrary. For $g = 1.0$, the lowest peak is at 2.39 MeV corresponding to the lowest 1^+ state in ^{48}Sc.

We note that these distributions are obtained after 15 Lanczos iterations (where $M^{2\nu}$ has converged) but the higher energies may fragment their strengths to nearby energies and thus may not correspond to physical states.

One sees that in the physical case ($g = 1.0$) there are considerable cancellations coming from the higher states. These cancellations decrease towards the negative g values and at $g = -1.0$ there is a coherent build up of the various contributions resulting in a large value of $M^{2\nu}$. Also, only the first few states contribute to the matrix element for all these g values indicating that the convergence of the 2ν strength is relatively fast, at least in the case of ^{48}Ca.

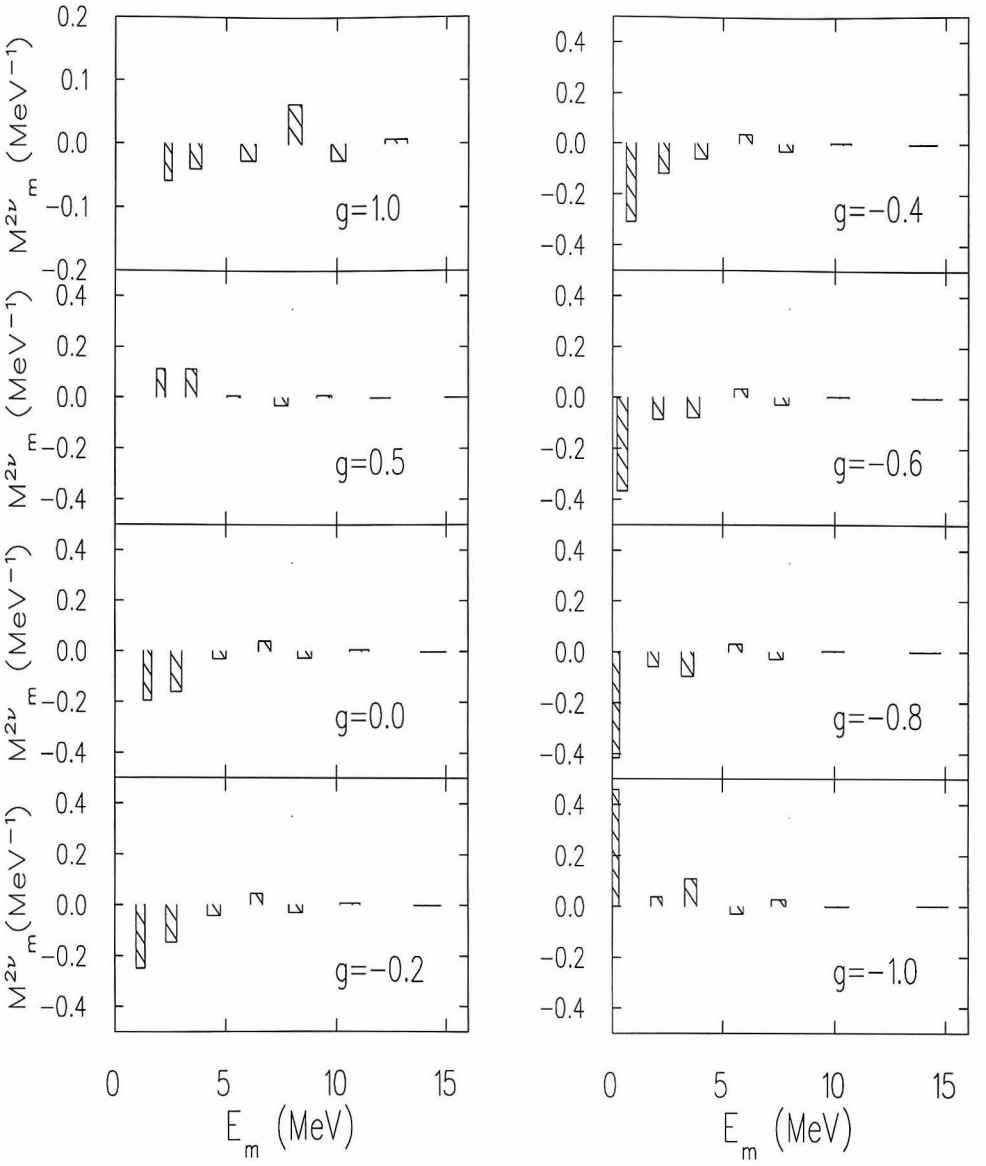

Figure 4.10: Contributions from the various 1^+ states in ^{48}Sc to the 2ν matrix element for the various g values obtained from direct-diagonalization.

4.4 Case of ^{76}Ge

As mentioned in section 2.5 the best limits on the 0ν decay have been obtained from the decay of ^{76}Ge. Hence, a comparison of the nuclear structure for the 2ν decay would be especially significant for the extraction of the neutrino mass from this limit.

Hence, we apply the SMMC method to this heavier nucleus, where direct diagonalization is not possible. We calculate the 2ν matrix element for ^{76}Ge using an effective interaction based on the Paris potential in the $(0f_{5/2}, 1p, 0g_{9/2})$ orbitals, with the single particle energies taken from the levels of ^{57}Ni relative to the ^{56}Ni core [63]. The model space comprises some 10^8 configurations, so that our SMMC calculation is significantly larger than previous shell model treatments of ^{76}Ge [9]. While it avoids spurious excitations of the center of mass, it does not include all spin-orbit pairs of orbitals and thus does not obey the Ikeda sum rule for GT strengths. However, this model space (with the choice of an appropriate effective interaction) should adequately describe those low-lying states expected to be the most important for $2\nu\beta\beta$ decay [82].

4.4.1 The interaction

The effective interaction has been constructed using a G-matrix folded-diagram method, in close analogy with the calculations carried out by Shurpin *et al.* [83] and by Dean *et al.* [27, 84] and contains atmost two-body terms. Three-body effects are known to be important for obtaining the saturation properties of nuclear matter [85] but are usually neglected in shell model calculations. Good agreement with experiment in various nuclear properties is usually obtained with "optimal" effective interactions for the lighter nuclei that have been studied in realistic model

spaces [27, 28]. While three-body interactions can in principle be included in direct-diagonalization calculations, the SMMC cannot incorporate them as then it becomes unamenable to the Hubbard-Stratonovich transformation.

There are a number of quantities that can, in principle, provide useful tests of the effective interaction. As one necessary (but not sufficient) test of the interaction, the energies of the neighboring $A = 76$ isobars relative to ^{76}Ge (the experimental values are Coulomb corrected following Ref. [68]) can be used; the results are shown in Table 4.3. We obtain the correct mass splittings to within 3 MeV indicating that some pieces of the interaction, at the very least, are reasonable. Note that the energy release of the ^{76}Ge decay, *i.e.* the mass splitting between ^{76}Ge and ^{76}Se is reproduced well with this interaction.

This calculation will underestimate the $B(E2)$ strengths, as this model space lacks strength coming from for instance, the coupling of the $f_{7/2}$ and $p_{3/2}$ by the quadrupole operator. Hence, a comparison with experiment is not possible for this quantity.

Our value for the β^- strength of ^{76}Ge is $B(GT_-) = \langle \mathbf{G}^\dagger \cdot \mathbf{G} \rangle = 19.09 \pm 0.39$ and we find an energy centroid of 6.3 ± 0.2 MeV, while the experimental values are 19.9 and 9.1 MeV respectively [86]; the apparent near consistency of this total strength with experiment is misleading as we have not employed the renormalization of $g_A = 1.0$ and we have missing strength in our model space corresponding mainly to the transitions between the $g_{9/2}$ and $g_{7/2}$ orbitals. This missing high-energy strength should not affect the low-lying states of ^{76}As that are important for $2\nu\beta\beta$ decay. Our value for the β^+ strength for ^{76}Se, $B(GT_+) = 0.60 \pm 0.13$. Unlike the case of ^{48}Ti, this strength is identically zero in the independent particle model and it is generated only by the smearing of the fermi surface due to the interaction.

Table 4.3: Masses of some $A = 76$ nuclei with respect to ^{76}Ge compared to experiment

nucleus	SMMC	Experiment
^{76}Zn	31.54 ± 0.25	28.35
^{76}Se	-21.35 ± 0.28	-20.72
^{76}Kr	-34.13 ± 0.46	-34.33
^{76}Sr	-38.30 ± 0.22	-39.90

4.4.2 2ν decay

We perform the ^{76}Ge calculation at $\beta = 2.5$ MeV^{-1} with $N_t = 60$. While at this temperature ^{76}Ge is not in its ground state (experimentally the first excited state is at 0.5 MeV and the extrapolated value of $\langle J^2 \rangle$ from the SMMC calculation is, $\langle J^2 \rangle = 2.1 \pm 1.2$ indicating an admixture of about $(35 \pm 20)\%$ for a two-state system with $J^\pi = 2^+$ as the first excited state). Calculations at higher temperature (which are feasible within the SMMC) suggest that temperature dependent effects for the relevant quantities $B(GT_+)$ of ^{76}Se, M_c, and $M^{2\nu}$ are negligible. Finite temperatures studies in the lower pf-shell nuclei on the total strengths [60] and the strength functions [64] seem to indicate that there is very little movement in these quantities for temperatures less that about 1 MeV even for nuclei where the first excited state is at energies typical of ^{76}Ge or ^{76}Se.

We perform two independent sets of calculations for both the closure and the exact matrix element using the $\chi = 4$ and $\chi = \infty$ families of $H(g, \chi)$. The best-fit extrapolations to $g = 1.0$ are linear for both the closure and the exact matrix elements in both cases. Our results for the closure matrix elements are -0.36 ± 0.34 and 0.08 ± 0.17 for $\chi = 4$ and $\chi = \infty$ respectively (shown in Fig. (4.11). These are to be compared with the truncated shell model calculation of Haxton *et al.*

[9] (using a different effective interaction) that resulted in a value of 2.56 and the more recent truncated shell model calculation [31] with yet another different effective interaction (see section 2.3) which one obtains a value of 0.68.

We find consistent $M^{2\nu}$ values for the $\chi = 4$ and $\chi = \infty$ cases (Fig. (4.12)). Our results are $0.12 \pm 0.07\ \mathrm{MeV}^{-1}$ and $0.12 \pm 0.06\ \mathrm{MeV}^{-1}$ respectively (a combined value of $0.12 \pm 0.05\ \mathrm{MeV}^{-1}$). That the completely independent $\chi = \infty$ and $\chi = 4$ calculations for $M^{2\nu}$ in ^{76}Ge lead to consistent $g = 1$ results gives us further confidence in that value. The experimental value of this matrix element (using $g_A = 1.26$) is $0.14 \pm 0.01\ \mathrm{MeV}^{-1}$ [14]. However, shell model calculations of ordinary β-decay consistently suggest that g_A is renormalized to 1.0 in the nuclear medium [27, 84], in which case the experimental matrix element is $0.22 \pm 0.01\ \mathrm{MeV}^{-1}$. The shell model calculation of Ref. [42] obtains a value of 0.15 for this matrix element.

Haxton *et al.* [9] obtained an estimate in the closure approximation by taking the average energy denominator to be the position of the β^- GT resonance in ^{76}Ge (9.4 MeV). We find significantly smaller values of $\bar{E} \equiv M_c/M^{2\nu}$ (-3.0 ± 3.3 MeV and 0.57 ± 1.26 MeV for $\chi = 4$ and ∞, respectively), in agreement with other $2\nu\beta\beta$ decay candidates such as ^{48}Ca, ^{100}Mo, and ^{128}Te where $\bar{E}$ is known to be significantly smaller than the position of the β^- GT resonance [82]. The more recent truncated shell model calculation of Caurier *et al.* [31] obtains a value of 4.82 for $\bar{E}$.

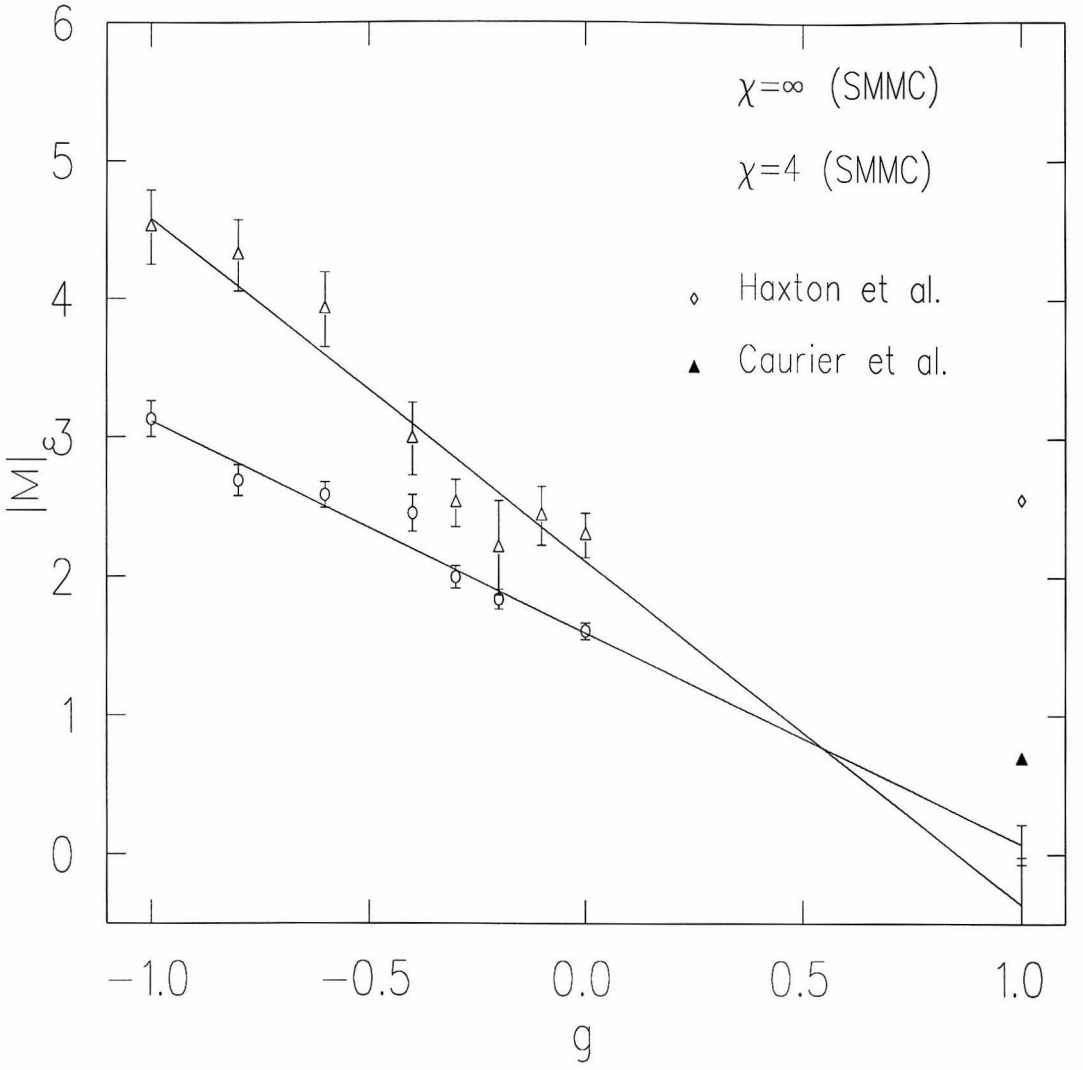

Figure 4.11: SMMC closure matrix elements for ^{76}Ge for $\chi = 4$ and $\chi = \infty$. The SMMC points are linearly extrapolated to $g = 1.0$.

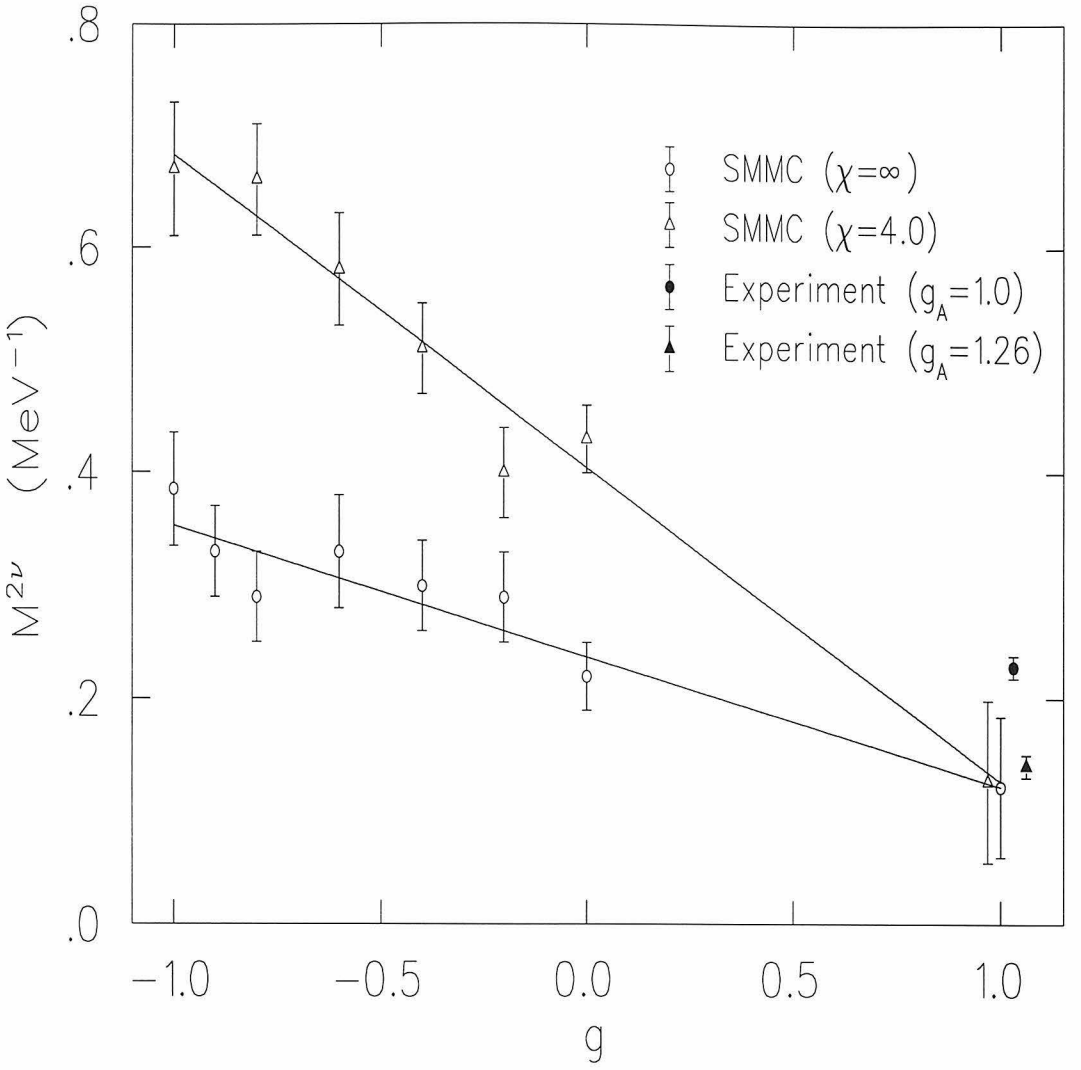

Figure 4.12: SMMC exact matrix elements for ^{76}Ge calculated using the Hamiltonians $H(g, \chi)$ with $\chi = 4$ and $\chi = \infty$. The lines are linear fits to the points in both cases. The extrapolated values and the experimental result of Ref. [14] are shown staggered around $g = 1.0$ for clarity.

Chapter 5 Summary and Conclusion

Double beta decay is the only test for the Majorana nature of neutrinos. Currently, there are several ongoing or planned experiments searching for 0ν decays. Two-neutrino double beta decay provides a sensitive test of nuclear structure that is relevant for zero-neutrino decay. However, being highly suppressed, the matrix element for the latter decay is difficult to calculate reliably.

In this thesis, an approach to the 2ν matrix element involving a four-body operator has been demonstrated using the Shell Model Monte Carlo. The method has been validated against direct-diagonalization methods for one of the lightest $\beta\beta$ candidates, ^{48}Ca. The first untruncated shell model calculation for the 2ν decay matrix element for ^{76}Ge in a realistic model space has been presented and the result is in reasonable agreement with experiment.

As with any application employing the SMMC, some uncertainty stems from possible unknown systematic errors due to the g-extrapolation, a necessary procedure to perform calculations with realistic interactions. One necessary test is to perform independent g dependent calculations from which to extrapolate to the physical results and this has been tested successfully for our result. A solution to the "sign problem" will greatly alleviate such uncontrollable errors (and will probably allow for much faster computation as the problem-free case will not require the exptrapolation).

The biggest uncertainty in this calculation (as in any nuclear structure calculation) stems from the choice of single-particle energies and the two-body interaction. The optimal interaction would derive from a G-matrix based interaction

with some tuning to describe nuclear properties correctly. Spectroscopy being an important ingredient of such optimizations is not possible for the heavier nuclei with the SMMC or any other scheme for solving the problem of A nucleons including direct-diagonlization. Thus, the question of optimal effective interactions for systems heavier than pf-shell nuclei remains an open one.

Using a direct diagonalization approach, it has been demonstrated in this thesis that even interactions that describe the relevant nuclear systems optimally can offer at least a factor of two in the nuclear matrix element for 2ν decay (and hence a factor of four in the half-life) upon a minor tuning of certain channels in the two-body interaction relevant for $\beta\beta$ decay. Contrary to the generally held belief, these matrix elements cannot be made arbitrarily small. In the process, one would destroy one's agreement of several other nuclear properties with experiment. Thus, the shell model (with the choice of the optimal effective interaction) can reproduce experimental half-lives and is not incapable of describing such weak second-order processes as $\beta\beta$ decay.

Also, in this thesis, a method for obtaining strength functions in nuclei has been demonstrated starting from response functions calculated within the SMMC. This method has been used to obtain Gamow-Teller strength functions for some nuclei participating in $\beta\beta$ decay and has been validated against direct-diagonalization. A detailed calculation of Gamow-Teller strength functions for other nuclei will be presented elsewhere from which electron capture rates on nuclei relevant to the presupernova evolution will be calculated.

Further studies in $\beta\beta$ decay using the SMMC will involve studies in heavier nuclei; ^{100}Mo and ^{128}Te are candidates where theoretical calculations will be useful to understand features like cancellations in the 2ν matrix element and this will be explored soon. Multi-major shell calculations will be an important ingredient to

these calculations and this technology being developed currently will be applied to such calculations.

SMMC can be applied to calculating the 0ν decay matrix elements. The intermediate virtual neutrino can have very high energies ($\simeq$ 100 MeV) compared to the excitation energies in the intermediate nucleus ($\simeq$ 10 MeV) making closure a good approximation in the calculation of the matrix elements. In addition, these matrix elements are less sensitive to certain channels in the nuclear interaction than the 2ν matrix element because the neutrino potential connects states of all possible angular momenta in the intermediate nucleus making the spin-isospin correlations less important to the sum. Since the range of the neutrino potential is of the order of the repulsive core, the short-range correlation need to be taken into account carefully. This can be done by multiplying the matrix element by some radial correlation function that accounts for the core. Using similar techniques of filtering out the ground state of the initial and final nucleus, the SMMC can thus be used to calculate the relevant matrix elements for this decay.

Bibliography

[1] M. Goeppert-Mayer, Phys. Rev. **48**, 512 (1935).

[2] S. Elliot, A. Hahn, and M. Moe, Phys. Rev. Lett **59**, 2020 (1987).

[3] W. Furry, Phys. Rev. **56**, 1184 (1939).

[4] R. Davis, Phys. Rev. **97**, 766 (1955).

[5] C. Wu *et al.*, Phys. Rev. **105**, 1413 (1957).

[6] H. Primakoff and S. Rosen, Rep. Prog. Phys. **22**, 121 (1959).

[7] B. Kayser, Comments Nucl. Part. Phys., 1985.

[8] C. Burgess and J. Cline, Phys. Rev. D **49**, 5925 (1994).

[9] W. C. Haxton and G. J. Stephenson, Prog. in Part. and Nucl. Phys. **12**, 409 (1984).

[10] F. Boehm and P. Vogel, *Physics of massive neutrinos* (Cambridge University Press, Cambridge, New York, 1987).

[11] P. Vogel, M. Ericson, and J. Vergados, Phys, Lett, B **212**, 259 (1988).

[12] D. Zheng, L. Zamick, and N. Auerbach, Phys. Rev. C **40**, 936 (1989).

[13] A. Balysh *et al.*, *TAUP*, 1995.

[14] A. Balysh *et al.*, Phys. Lett. B **322**, 176 (1994).

[15] S. Elliot *et al.*, Phys. Rev. C **46**, 1535 (1992).

[16] A. Kawashima, K. Takahashi, and A. Masuda, Phys. Rev. C **47**, 2452 (1993).

[17] H. Ejiri *et al.*, Phys. Lett. B **258**, 17 (1991).

[18] H. Ejiri *et al.*, J. Phys. Jpn. **64**, 339 (1995).

[19] T. Bernatowicz *et al.*, Phys. Rev. Lett. **69**, 2341 (1992).

[20] V. Artemiev *et al.*, JETP Lett. **58**, 262 (1993).

[21] A. Turkevich, T. Economou, and G. Cowan, Phys. Rev. Lett. **67**, 3211 (1991).

[22] L. Zamick and N. Auerbach, Phys. Rev. C **26**, 2185 (1982).

[23] J. Bernabeu *et al.*, Z. Phys. C **40**, 323 (1990).

[24] P. Vogel and W. Ormand, Phys. Rev. C **47**, 623 (1993).

[25] M. Mayer and J. Jensen, *Elementary theory of nuclear shell structure* (Wiley, New York, 1955).

[26] S. Cohen and D. Kurath, Nucl. Phys. **73**, 1 (1965).

[27] B. Brown and B. Wildenthal, Ann. Rev. Nucl. Part. Sci. **38**, 29 (1988).

[28] K. Langanke, D. J. Dean, P. B. Radha, Y. Alhassid, and S. E. Koonin, Phys. Rev. C **52**, 718 (1995).

[29] T. T. S. Kuo and G. E. Brown, Nucl. Phys. A **114**, 241 (1968).

[30] A. Poves and A. Zuker, Phys. Rep. **70**, 235 (1981).

[31] E. Caurier, F. Nowacki, A. Poves, and J. Retamosa, nucl-th/9601017 (1996).

[32] G. F. Bertsch and H. Esbensen, Rep. Prog. Phys. **50**, 607 (1987).

[33] K. Muto, E. Bender, and H. Kalpdor-Kleingrothaus, Z. Phys. A **339**, 435 (1991).

[34] E. Caurier, A. Poves, and A. Zuker, Phys. Lett. B **252**, 13 (1990).

[35] J. Engel, P. Vogel, and M. Zirnbauer, Phys. Rev. C **37**, 731 (1988).

[36] A. Garcia *et al.*, Phys. Rev. C **47**, 2910 (1993).

[37] J. Toivanen and J. Suhonen, Phys. Rev. Lett. **75**, 410 (1995).

[38] L. Zhao and B. Brown, Phys. Rev. C **47**, 2641 (1993).

[39] M. Moe and P. Vogel, Ann. Rev. Nucl. Part. Sci. **44**, 247 (1994).

[40] T. Tomoda, Rep. Prog. Phys. **54**, 53 (1991).

[41] B. Brown and B. Wildenthal, *At. Data. Nucl. Data Tables*, 1985.

[42] G. Martinez-Pinedo, A. Poves, E. Caurier, and A. P. Zuker, nucl-th/9603039 (1996).

[43] M. Rho, Nucl. Phys. A **231**, 493 (1974).

[44] K. Ohta and M. Wakamatsu, Phys. Lett. B **51**, 325 (1974).

[45] M. Inghram and J. Reynolds, Phys. Rev. **78**, 822 (1950).

[46] O. Manuel, J. Phys. G: Nucl. and Part. Phys. **17**, S221 (1991).

[47] B. Pontecorvo, Phys. Lett. B **26**, 630 (1968).

[48] J.-L. Vuilleumier, Phys. Rev. D **48**, 1009 (1993).

[49] M. Moe, Int. J. Mod. Phys. **E2**, 507 (1993).

[50] G. Lang, C. Johnson, S. Koonin, and W. Ormand, Phys. Rev. C **48**, 1518 (1993).

[51] S. Koonin, D. Dean, and K. Langanke, Phys. Rep. (1995).

[52] C. Johnson, S. Koonin, G. Lang, and W. Ormand, Phys. Rev. Lett. **69**, 3157 (1992).

[53] Y. Alhassid, D. J. Dean, S. E. Koonin, G. Lang, and W. E. Ormand, Phys. Rev. Lett. **72**, 613 (1994).

[54] W. Ormand, D. Dean, C. Johnson, G. Lang, and S. Koonin, Phys. Rev. C **C49**, 1422 (1994).

[55] J. Hubbard, Phys. Rev. Lett. **3**, 77 (1959).

[56] R. Stratonovich, Dokl. Akad. Nauk. SSSR **115**, 1097 (1957).

[57] N. Metropolis, A. Rosenbluth, M. Rosenbluth, A. Teller, and E. Teller, J. Chem. Phys. **21**, 1087 (1953).

[58] D. J. Dean, S. E. Koonin, G. Lang, W. E. Ormand, and P. B. Radha, Phys. Lett. B **317**, 275 (1993).

[59] Y. Alhassid, D. Dean, S. Koonin, G. Lang, and W. Ormand, Phys. Rev. Lett. **72**, 613 (1994).

[60] D. J. Dean, S. E. Koonin, K. Langanke, P. B. Radha, and Y. Alhassid, Phys. Rev. Lett **74**, 2909 (1995).

[61] E. Loh and J. Gubernatis, *Electronic Phase Transitions* (Elsevier Science Publishers B.V., New York, 1992).

[62] S. Meshkov and D. Berkov, Int. J. of Mod. Phys. **C5**, 987 (1994).

[63] A. Bohr and B. Mottelson, *Nuclear Structure* (W.A. Benjamin, Inc., New York, 1969), Vol. 1.

[64] P. B. Radha, D. J. Dean, S. E. Koonin, and K. Langanke, to be submitted to Phys. Rev. C.

[65] P. B. Radha *et al.*, Phys. Rev. Lett. **76**, 2642 (1996).

[66] A. Poves, P. B. Radha, K. Langanke, and P. Vogel, Phys. Lett. B **361**, 1 (1995).

[67] E. Caurier, A. Zuker, A. Poves, and G. Martinez-Pinedo, Phys. Rev. C **50**, 225 (1994).

[68] W. Myers and W. Swiatecki, Nucl. Phys. **81**, 1 (1966).

[69] W. Alford *et al.*, Nucl. Phys. A **514**, 49 (1990).

[70] B. Anderson *et al.*, Phys. Rev. C **31**, 1161 (1985).

[71] H. A. Bethe, G. E. Brown, J. Applegate, and J. M. Lattimer, Nucl. Phys. A **324**, 487 (1979).

[72] A. L. Williams *et al.*, Phys. Rev. C **51**, 1144 (1995).

[73] S. El-Kateb *et al.*, Phys. Rev. C **49**, 3129 (1994).

[74] J. Rapaport *et al.*, Nucl. Phys. A **410**, 371 (1983).

[75] B. D. Anderson *et al.*, Phys. Rev. C **41**, 1474 (1990).

[76] G. M. Fuller, W. A. Fowler, and M. J. Newman, Astrophysical Journal **293**, 1 (1985).

[77] E. Caurier, *code ANTOINE*, Strasbourg, 1989.

[78] R. Bardin *et al.*, Nucl. Phys. A **158**, 337 (1970).

[79] K. Ogawa and H. Horie, edited by M. Morita *et al.* (World Scientific, Singapore, 1989), p. 308.

[80] L. Zhao, B. Brown, and W. Richter, Phys. Rev. C **42**, 1120 (1990).

[81] K. Kumar and M. Baranger, Nucl. Phys. A **110**, 490 (1968).

[82] M. Ericson, T. Ericson, and P. Vogel, Phys. Lett. B **328**, 259 (1994).

[83] J. Shurpin, T. Kuo, and D. Strottman, Nucl. Phys. A **408**, 310 (1983).

[84] D. J. Dean, S. E. Koonin, T. Kuo, K. Langanke, and P. B. Radha, Phys. Lett. B **367**, 17 (1996).

[85] J. W. Negele, Phys. Rev. C **1**, 1260 (1970).

[86] R. Madey *et al.*, Phys. Rev. C **40**, 540 (1989).